T CELL MEMORY

Early precursors and molecular determinants of tissue-resident memory CD8⁺ T lymphocytes revealed by single-cell RNA sequencing

Nadia S. Kurd[1]*[†], Zhaoren He[2,3]*, Tiani L. Louis[1], J. Justin Milner[3], Kyla D. Omilusik[3], Wenhao Jin[2], Matthew S. Tsai[1], Christella E. Widjaja[1], Jad N. Kanbar[1], Jocelyn G. Olvera[1], Tiffani Tysl[1], Lauren K. Quezada[1], Brigid S. Boland[1], Wendy J. Huang[2], Cornelis Murre[3], Ananda W. Goldrath[3], Gene W. Yeo[2,4‡], John T. Chang[1,5‡§]

During an immune response to microbial infection, CD8⁺ T cells give rise to distinct classes of cellular progeny that coordinately mediate clearance of the pathogen and provide long-lasting protection against reinfection, including a subset of noncirculating tissue-resident memory (T_RM) cells that mediate potent protection within nonlymphoid tissues. Here, we used single-cell RNA sequencing to examine the gene expression patterns of individual CD8⁺ T cells in the spleen and small intestine intraepithelial lymphocyte (siIEL) compartment throughout the course of their differentiation in response to viral infection. These analyses revealed previously unknown transcriptional heterogeneity within the siIEL CD8⁺ T cell population at several stages of differentiation, representing functionally distinct T_RM cell subsets and a subset of T_RM cell precursors within the tissue early in infection. Together, these findings may inform strategies to optimize CD8⁺ T cell responses to protect against microbial infection and cancer.

INTRODUCTION

CD8⁺ T cells responding to microbial challenge differentiate into distinct subsets of cellular progeny with unique migratory and functional properties that coordinately mediate clearance of the pathogen (effector cells) and provide long-lasting protection against reinfection (memory cells). Considerable heterogeneity has been previously described within the long-lived circulating memory T cell pool (1–3). Whereas central memory (T_CM) cells exhibit greater self-renewal and plasticity with the ability to rapidly proliferate and differentiate into secondary effector cells upon reinfection, effector memory (T_EM) cells provide immediate pathogen control via rapid and potent "effector" function. Moreover, recent studies have revealed additional heterogeneity within the classically defined T_EM cell population, including long-lived effector (LLE) cells and peripheral memory cells, which can be distinguished by distinct surface molecule expression and trafficking properties (1, 2, 4–6). In addition to these circulating memory T cell populations, a noncirculating subset, termed tissue-resident memory (T_RM) cells, has recently been described (7). T_RM cells are found in most tissues and positioned at key barrier surfaces, such as the skin and intestinal epithelium, where they play critical roles in limiting early pathogen spread and controlling infection, and also help to control the outgrowth of cancer cells (8–11). Whereas heterogeneity within the circulating CD8⁺ T cell memory population has been well characterized, it remains unclear whether the tissue-resident CD8⁺ T cell population might also be composed of distinct subsets that play unique roles in mediating protective immunity.

Recent studies have begun to illuminate the mechanisms regulating T_RM cell differentiation, function, and survival. Activation of naïve CD8⁺ T cells occurs in the spleen or draining lymph nodes, resulting in the up-regulation of key transcription factors including Blimp-1 (12). Recruitment of activated CD8⁺ T cells to nonlymphoid tissue sites is mediated by chemokine receptors that promote tissue entry, such as CCR9 and CXCR3 (12–14). Upon entry to tissue, CD8⁺ T cells undergo transcriptional changes that enforce tissue residency, in part by dampening expression of receptors that promote return to circulation such as CCR7 and S1PR1 (14), and begin to direct the T_RM cell differentiation program. These changes include up-regulation of transcription factors such as Hobit, which, together with Blimp-1, repress genes associated with recirculation, including *Klf2*, *S1pr1*, and *Ccr7*; and down-regulation of the T-box transcription factors T-bet and Eomes, enabling transforming growth factor–β (TGF-β) responsiveness (12–15). TGF-β signals within the tissue induce expression of CD103, a key factor for tissue retention, whereas low levels of T-bet expression are required for interleukin-15 (IL-15) responsiveness, which plays an important role for long-term survival of T_RM cells in some tissues (13, 15). However, additional unidentified regulators likely contribute to coordinating the T_RM cell differentiation program. Moreover, although it has been shown that T_RM cells preferentially arise from circulating precursors with low expression of killer cell lectin like receptor G1 (KLRG1) (13, 16), it remains unknown whether all cells that enter the tissue are destined to persist and continue their differentiation into T_RM cells or whether T_RM cells are derived from a specific subset of precursors within the tissue at early time points.

Several studies have described a core transcriptional signature that is shared among T_RM cells from distinct tissues, highlighting several key transcriptional regulators of T_RM cell differentiation, including Hobit, Blimp-1, and Runx3 (12, 16–19). However, most of these prior studies have focused on relatively late time points after the T_RM cell population has been well established, providing

[1]Department of Medicine, University of California San Diego, La Jolla, CA, USA. [2]Department of Cellular and Molecular Medicine, University of California San Diego, La Jolla, CA, USA. [3]Division of Biologic Sciences, University of California San Diego, La Jolla, CA, USA. [4]Institute for Genomic Medicine, University of California San Diego, La Jolla, California, USA. [5]Division of Gastroenterology, VA San Diego Healthcare System, San Diego, CA, USA.
*These authors contributed equally to this work.
†Present address: Cancer Immunology Discovery, Pfizer Oncology Research and Development, La Jolla, CA 92121, USA.
‡Corresponding author. Email: geneyeo@ucsd.edu (G.W.Y.); changj@ucsd.edu (J.T.C.)
§Lead contact.

only a snapshot of the gene expression patterns used by T_RM cells and potentially missing early events important for their differentiation. Moreover, because these studies relied on RNA sequencing of bulk cell populations, potential heterogeneity representing distinct functional subsets or intermediate states of differentiation may have been missed.

Single-cell RNA sequencing (scRNA-seq) is a powerful approach that can reveal heterogeneity within cell populations and has been used extensively in recent studies to probe the dynamic gene expression patterns within a wide range of immune cell types in health and disease (20–29). This approach has allowed for the elucidation of new cell subsets and states, such as highly efficacious subpopulations of tumor-infiltrating lymphocytes and early states of differentiation for circulating effector and memory CD8+ T cells (20, 22, 23). Here, we used scRNA-seq to generate a single-cell transcriptomic dataset elucidating the dynamic gene expression patterns of individual CD8+ T cells in the spleen and small intestine intraepithelial lymphocyte (siIEL) compartment throughout the course of their differentiation in response to viral infection. These analyses demonstrate that the circulating and tissue-resident subtypes of memory CD8+ T cells use highly overlapping patterns of gene expression, revealing a core transcriptional program used by both subtypes throughout their differentiation. In addition, these analyses elucidated sets of genes with kinetics and expression patterns unique to circulating or T_RM CD8+ T cells that may contribute to the specification of each distinct subtype. These data also revealed transcriptional heterogeneity within the siIEL CD8+ T cell population throughout its differentiation. We show that within the established T_RM cell population, this molecular heterogeneity reflects functionally distinct subsets that were previously unknown. Moreover, we identify a distinct subset within the CD8+ T cell pool within the tissue early in infection that likely represents the precursors of T_RM cells. These findings should inform future studies aimed at improving our understanding of T_RM cell differentiation and function, which may contribute to our ability to better manipulate CD8+ T cell responses to protect against infection and cancer.

RESULTS

scRNA-seq analyses of circulating and siIEL CD8+ T cells responding to viral infection

We used a scRNA-seq approach to investigate the transcriptional changes that occur in circulating and siIEL CD8+ T cells responding to viral infection. We adoptively transferred P14 CD8+CD45.1+ T lymphocytes, which have transgenic expression of a T cell receptor (TCR) that recognizes an immunodominant epitope of lymphocytic choriomeningitis virus (LCMV), into congenic CD45.2+ wild-type (WT) recipients that were infected with the Armstrong strain of LCMV 1 day later. We FACS (fluorescence-activated cell sorting)–sorted naïve (CD62L^hi CD44^lo) P14 T cells from spleens of uninfected mice and activated donor P14 T cells (CD44^hi) from the spleens and siIEL compartments of recipient mice at 11 time points after infection and performed scRNA-seq using the 10x Genomics Chromium platform (Fig. 1A and fig. S1).

To relate changes in CD8+ T cell populations over time and across tissues, we merged the data from all time points and anatomic sites and performed unsupervised t-distributed stochastic neighborhood embedding (tSNE) and uniform manifold approximation and projection (UMAP) analyses (Fig. 1, B to D, and fig. S2). CD8+

T cells from the siIEL compartment clustered distinctly from splenic CD8+ T cells at all time points (Fig. 1, B to D, and fig. S2), consistent with the distinct transcriptional profile of T_RM cells that has been previously reported (12, 13, 16, 18, 19). For example, expression of genes previously associated with T_RM cells, such as Cd69 and Itgae, was strongly enriched among siIEL CD8+ T cells compared with splenic CD8+ T cells, whereas expression of genes that promote tissue egress and recirculation, such as Klf2 and S1pr1, was strongly enriched among splenic cells compared with siIEL cells (Fig. 1E). The divergence in gene expression profiles between splenic and siIEL CD8+ T cells was evident as early as day 4 after infection (Fig. 1, B to D, and fig. S2), the earliest time point at which CD8+ T cells can be detected within the intestinal epithelium (30), indicating that CD8+ T cells begin to change their transcriptional profile rapidly upon entry into tissue. Differential expression analyses revealed that 928 genes were more highly expressed in day 4 splenic CD8+ T cells and 1103 genes were more highly expressed in day 4 siIEL CD8+ T cells, including Cd69 and Itgae (Fig. 1, E and F; fig. S3; and table S1). Genes more highly expressed by siIEL CD8+ T cells included those associated with processes known to be important for establishment and maintenance of T_RM cells, including integrins and cell adhesion molecules (Itga1, Itgb2, Itgal, Itgb7, Itgax, and Jaml), regulators of cell trafficking (Ccr9 and Cxcr3) and TGF-β signaling (Tgif1, Tgfbr2, Smad7, Skil, and Smurf2), the tissue damage receptor P2xr7 (31), and fatty acid–binding proteins (Fabp1, Fabp2, and Fabp6) (Fig. 1F, fig. S3, and table S1) (32). In addition, genes associated with other aspects of T cell function, including cytokines (Il2 and Il10), cytokine receptors (Il4ra, Il2rg, Il10rb, and Il21r), chemokines (Ccl3, Ccl4, Ccl5, Cxcl10, and Cxcl11), effector molecules (Gzma, Gzmk, and Fasl), and both costimulatory (Icos and Cd28) and inhibitory (Ctla4, Tigit, and Lag3) receptors, were more highly expressed by siIEL CD8+ T cells. We also observed that genes encoding components and downstream mediators of the TCR signaling pathway (Zap70, Itk, Lats2, Rasgrp1, Fyb, Nr4a1, Nr4a2, Nfatc1, Irf4, Ikzf2, and Cd5), regulators of intracellular calcium (Orai1, Orai2, Sri, and Rrad), and regulators of nuclear factor κB (NF-κB) signaling (Nfkbia, Nfkbiz, Rel, Ikbkb, Pim1, and Tnfaip3) were more highly expressed among siIEL CD8+ T cells. Many of these differentially expressed (DE) genes were transcription factors with no previously reported role in T_RM cells (Ikzf2, Ikzf3, Gata3, Irf4, and Id2). Among the genes more highly expressed by splenic CD8+ T cells were Batf and Zeb2, transcription factors that have been shown to regulate effector CD8+ T cell differentiation (33, 34); genes encoding for transcription factors, such as Batf3, that have not been previously implicated in CD8+ T cell differentiation; and genes encoding the high-affinity IL-2 receptor (IL-2Rα) and the OX40 costimulatory receptor (Fig. 1F, fig. S3, and table S1). Thus, these analyses reveal previously unappreciated signaling pathways and transcription factors that may represent early regulators of circulating versus siIEL CD8+ T cell differentiation.

Gene ontology (GO) analyses revealed that genes associated with DNA replication and cell cycle regulation were enriched among splenic CD8+ T cells, suggesting that siIEL CD8+ T cells may be less proliferative than splenic CD8+ T cells (table S1). Assessment of cell cycle status inferred from transcriptional analyses suggested that although both splenic and siIEL CD8+ T cells were actively dividing at day 4 after infection, siIEL CD8+ T cells had stopped proliferating by day 7 after infection, whereas splenic CD8+ T cells continued proliferating until 7 to 10 days after infection (Fig. 1G).
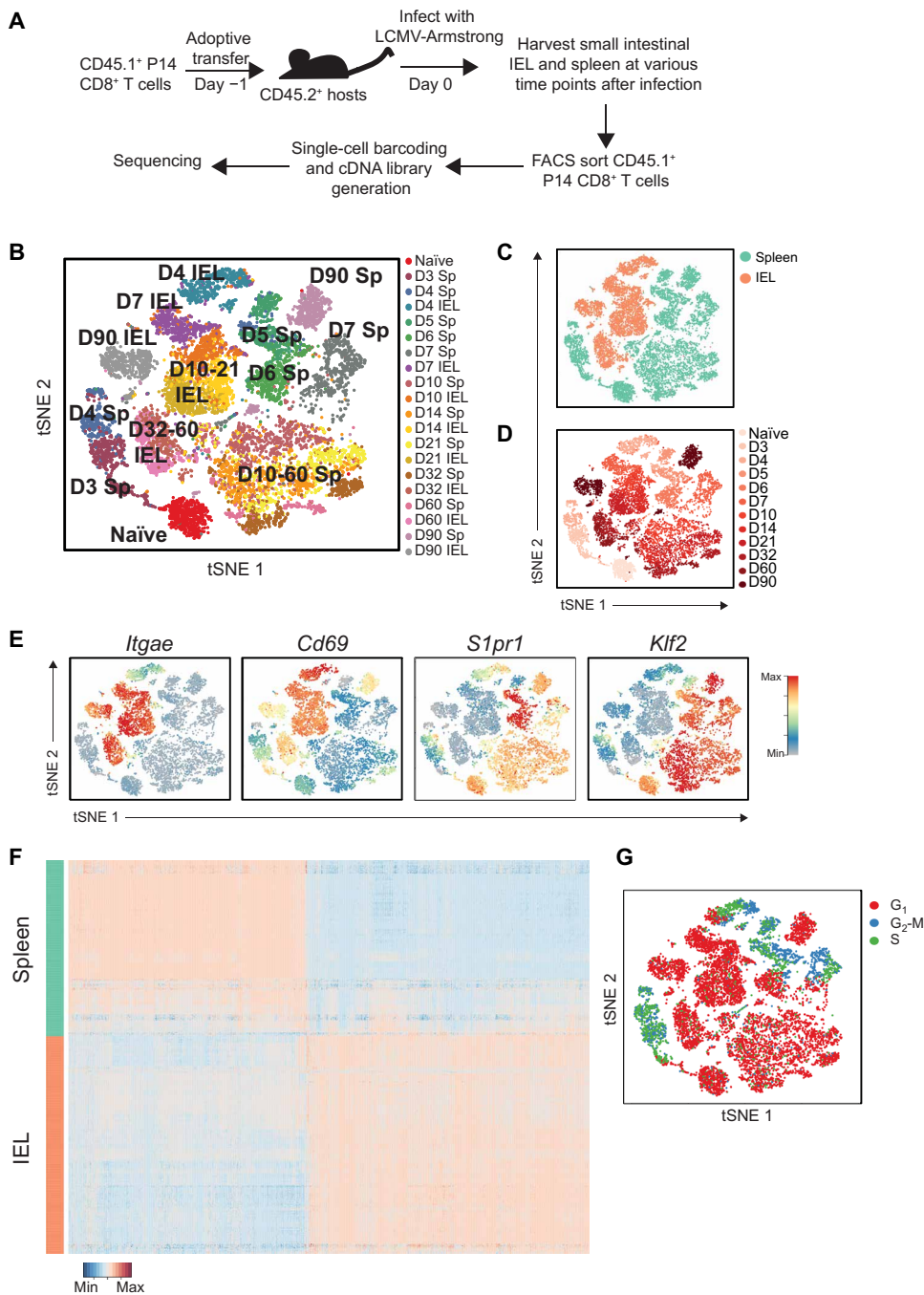
Fig. 1. scRNA-seq analyses of circulating and siIEL CD8+ T cells responding to viral infection. (**A**) Experimental setup. P14 CD45.1+CD8+ T cells were adoptively transferred into congenic CD45.2+ hosts 1 day before infection with LCMV-Armstrong. Splenocytes were harvested at 3, 5, and 6 days; splenocytes and siIEL CD8+ T cells were harvested at 4, 7, 10, 14, 21, 32, 60, and 90 days after infection. Naïve T cells (CD44loCD62Lhi) were harvested from spleens of uninfected P14 TCR transgenic mice. Antigen-experienced P14 CD8+ T cells (CD45.1+Vα2+CD44hi) were sorted and processed for scRNA-seq with the 10x Genomics platform. cDNA, complementary DNA. (**B** to **D**) tSNE analysis of all scRNA-seq samples, where each individual sample (B), tissue (C), or time point (D) is represented by a unique color. (**E**) Relative expression of known regulators of circulating memory and T_{RM} CD8+ T cell differentiation superimposed on individual cells. (**F**) Differential gene expression in day 4 splenic (teal) and siIEL (coral) CD8+ T cells, represented as expression relative to the mean expression among all cells; each row represents an individual cell, and each column represents an individual gene. Threshold for DE genes was $P < 0.05$ (two-sided Wilcoxon test) and an absolute fold change of >2. (**G**) Cell cycle status of individual CD8+ T cells, inferred from transcriptional profiles.

These findings indicated that siIEL CD8+ T cells become quiescent more rapidly after activation compared with splenic CD8+ T cells. Together, these data reveal that CD8+ T cells that enter the siIEL compartment receive signals that alter their transcriptional profile rapidly after arrival, indicating that the T_{RM} cell fate may begin to be specified earlier than previously appreciated and may serve as a useful resource for identifying early molecular determinants of T_{RM} cell differentiation.

Shared and tissue-specific components of gene expression programs in circulating and siIEL CD8+ T cells

We next sought to elucidate changes in gene expression programs over time in CD8+ T cells responding to viral infection and to understand how gene expression programs in circulating versus siIEL CD8+ T cells relate to one another. We analyzed splenic and siIEL CD8+ T cells separately and performed weighted gene coexpression network analyses on each set of cells, defining tissue-specific modules of genes that exhibited similar patterns of expression over time in splenic (fig. S4, A and B, and table S2) or siIEL (fig. S4, C and D, and table S2) CD8+ T cells. We identified 10 and 8 distinct gene expression modules among splenic and siIEL CD8+ T cells, respectively (fig. S4, A to D, and table S2).

Although recent studies have primarily highlighted the differences in gene expression between circulating and tissue-resident CD8+ T cells (*12, 13, 16, 18, 19*), we found substantial overlap in the gene expression patterns used by differentiating splenic and siIEL CD8+ T cells. For example, 38% of the genes in Spleen Module 1 were shared with IEL Module 2; genes in these early differentiation modules were characterized by a decrease in expression, relative to that by naïve cells, after T cell activation (fig. S4, B, D, and E). Similarly, 40% of the genes in IEL Module 4 were shared with Spleen Module 4; genes in these intermediate differentiation modules were characterized by high expression during the peak of infection, followed by a subsequent decrease. Last, 33% of the genes in IEL Module 7 were shared with Spleen Module 10; genes in these late differentiation modules were characterized by a

reduction in expression after T cell activation, followed by increasing expression that was sustained at late time points (fig. S4, B, D, and E, and table S2). These observations suggested that splenic and siIEL CD8$^+$ T cells share a core transcriptional program throughout their differentiation, consistent with their common cytolytic lymphocyte functions (fig. S4E and table S2), and highlight the potential value of this dataset to reveal how specific genes or pathways, including those known to play key roles in regulating circulating memory CD8$^+$ T cells, may act similarly or disparately in regulating T$_{RM}$ cell differentiation.

To elucidate distinct regulators of the circulating memory and T$_{RM}$ cell differentiation programs, we again performed weighted gene coexpression network analyses but, this time, analyzed splenic and siIEL CD8$^+$ T cells together. This approach enabled us to directly compare the level of representation of each module in cells from each anatomic site at each time point. Fifteen modules representing distinct temporal patterns of gene expression were defined and annotated as Combined Modules 1 to 15 (Fig. 2, A to C, and table S3). This analysis confirmed our observation that splenic and siIEL CD8$^+$ T cells share a core transcriptional program, as many Combined Modules were similarly represented in splenic and siIEL CD8$^+$ T cells throughout most of their differentiation (Fig. 2, B and C). Moreover, this analysis confirmed our finding that siIEL CD8$^+$ T cells were transcriptionally distinct from splenic CD8$^+$ T cells as early as day 4 after infection (Fig. 1, B to F), because we noted that many modules (Combined Modules 2, 3, 5, 7, 11, and 12) were differentially represented within splenic and siIEL CD8$^+$ T cells at day 4 after infection but not at later time points (Fig. 2, B and C). For example, genes in one such module, Combined Module 12, were enriched in several pathways known to play roles in circulating CD8$^+$ T cell memory cells, including autophagy, protein ubiquitination, and proteasome protein catabolism (table S3) (35, 36). These findings suggested that differentiating siIEL CD8$^+$ T cells may begin to acquire certain aspects of a memory-like transcriptional profile more rapidly than splenic CD8$^+$ T cells.

These analyses also defined several modules that were significantly and consistently differentially enriched in splenic versus siIEL CD8$^+$ T cells over time. For example, Combined Modules 6 and 15 were enriched in siIEL compared with splenic CD8$^+$ T cells; genes in these modules were highly up-regulated in siIEL CD8$^+$ T cells throughout their differentiation (Fig. 2, B and C). Combined Modules 6 and 15 contained 157 and 371 genes, respectively, some of which have been previously implicated in CD8$^+$ T$_{RM}$ cell differentiation and function, such as *Cd69*, *Itgae*, *Itga1*, and *Ccr9*, which regulate homing and retention within the intestinal environment; transcription factors *Nr4a1* and *Ahr*, which regulate the long-term maintenance of T$_{RM}$ (37, 38), *Runx3*, a transcriptional regulator of key genes that establish tissue residency that is critical for T$_{RM}$ cell differentiation (16), and *Bhlhe40*, which sustains T$_{RM}$ cell metabolic fitness and promotes an epigenetic state permissive for expression of key tissue residency genes (39); and *Ccl3* and *Ccl4*, which are involved in the rapid recruitment of innate cells by T$_{RM}$ cells (Fig. 2D, fig. S5, and table S3) (8, 10). In addition, GO analyses revealed enrichment of pathways known to play roles in T$_{RM}$ cell differentiation and maintenance, such as TGF-β signaling (15) (*Skil*, *Smurf*, and *Tgif1*) and fatty acid homeostasis (*Dgat1* and *Got1*), consistent with the dependence of T$_{RM}$ cells on fatty acid metabolism for their maintenance and function (Fig. 2D, fig. S5, and table S3) (32). These T$_{RM}$ cell–enriched modules also included genes encoding effector

molecules and cytokines, such as *Il2*, *Ifng*, *Tnf*, *Fasl*, and *Gzmb*, sustained high expression of which may contribute to the rapid and potent recall responses of T$_{RM}$ cells. Moreover, other groups of genes represented in these modules implicated pathways with previously unexplored roles in T$_{RM}$ cell differentiation, some of which were already up-regulated in siIEL CD8$^+$ T cells as early as day 4 after infection (Fig. 1F and fig. S3). These included inhibitory receptors (*Ctla4*, *Lag3*, *Cd101*, and *Tigit*), factors involved in TCR signaling and costimulation (*Zap70*, *Lat*, *Cd8a*, *Cd3e*, *Cd40lg*, and *Nfatc1*), regulators of cell survival (*Bcl2a1b*, *Bcl2l11*, and *Bcl2a1d*) and NF-κB signaling (*Nfkbia*, *Nfkbiz*, *Nfkbid*, and *Rel*), genes involved in cytokine responses (*Stat3*, *Stat1*, *Irak2*, *Socs1*, and *Jak2*), and transcription factors with previously uncharacterized roles in T$_{RM}$ cell differentiation (*Nr4a2*, *Nr4a3*, *Junb*, *Fosl2*, *Tox*, *Foxo3*, and *Irf4*) (Fig. 2D, fig. S5, and table S3). In addition, genes involved in cholesterol biosynthesis (*Fdps*, *Cyp51*, *Mvk*, *Fdft1*, *Hmgcr*, and *Hmgcs*) and steroid hormone–mediated signaling pathways were enriched in Combined Modules 6 and 15, respectively, raising the possibility of a role for these processes in T$_{RM}$ cell differentiation.

By contrast, Combined Modules 8 and 9 were enriched in splenic relative to siIEL CD8$^+$ T cells beginning at day 7 after infection and included 196 and 138 genes, respectively, some of which have been previously implicated in promoting differentiation of circulating memory CD8$^+$ T cells at the expense of T$_{RM}$ cells (Fig. 2, B and C, and table S3). For example, these spleen-enriched modules included *Klf2*, *S1pr1*, *Ly6c1*, and *Ly6c2*, which regulate trafficking and egress, and *Eomes*, a transcription factor that negatively regulates T$_{RM}$ cell differentiation (fig. S5 and table S3) (12, 14, 15, 30). These spleen-enriched modules also included several cell surface markers, including *Cx3cr1* and *Klrg1*, that have been associated with subsets of circulating effector CD8$^+$ T cells. In addition, the presence of genes encoding specific cytokine receptors (*Il18r1*, *Il18rap*, and *Il17ra*) in these spleen-enriched modules suggests that signaling through these receptors might negatively regulate T$_{RM}$ cell differentiation and maintenance.

To demonstrate that genes identified by these analyses represent functionally important regulators of T$_{RM}$ cell differentiation, we selected for further studies three genes found in Combined Module 15, nuclear receptor subfamily 4 group A member 2 (*Nr4a2*), and two activating protein-1 (AP-1) transcription factor subunits, Junb proto-oncogene (*Junb*) and FOS-like 2 (*Fosl2*). These genes exhibited increased expression in siIEL relative to splenic CD8$^+$ T cells at all time points (Fig. 2D). *Nr4a2* is an orphan nuclear receptor that belongs to the Nr4a family of transcription factors, plays a central role in the development of regulatory T cells and pathogenic T helper 17 (T$_H$17) cells (40–43), and has been implicated as an important driver of exhaustion in CD8$^+$ T cells (44). *Junb* and *Fosl2* play important roles in regulating T$_H$17 cell identity and pathogenicity (45–47), and *Junb* has also been implicated as part of the effector CD8$^+$ T cell transcriptional program (34). *Nr4a2*, *Junb*, and *Fosl2* have not been previously reported to regulate the differentiation of T$_{RM}$ cells. To investigate whether these genes play a role in T$_{RM}$ cell differentiation, we transduced P14 CD8$^+$CD45.1$^+$ T cells with retroviruses encoding short hairpin RNA (shRNA) targeting *Nr4a2*, *Junb*, or *Fosl2* and transduced P14 CD8$^+$CD45.1.2$^+$ T cells with retroviruses encoding nontargeting shRNA. Cells were mixed at a 1:1 ratio and adoptively transferred into CD45.2 recipient mice that were subsequently infected with LCMV (fig. S6A). Relative to nontargeting controls, knockdown (KD) of *Nr4a2*, *Junb*, or *Fosl2* resulted in a greater
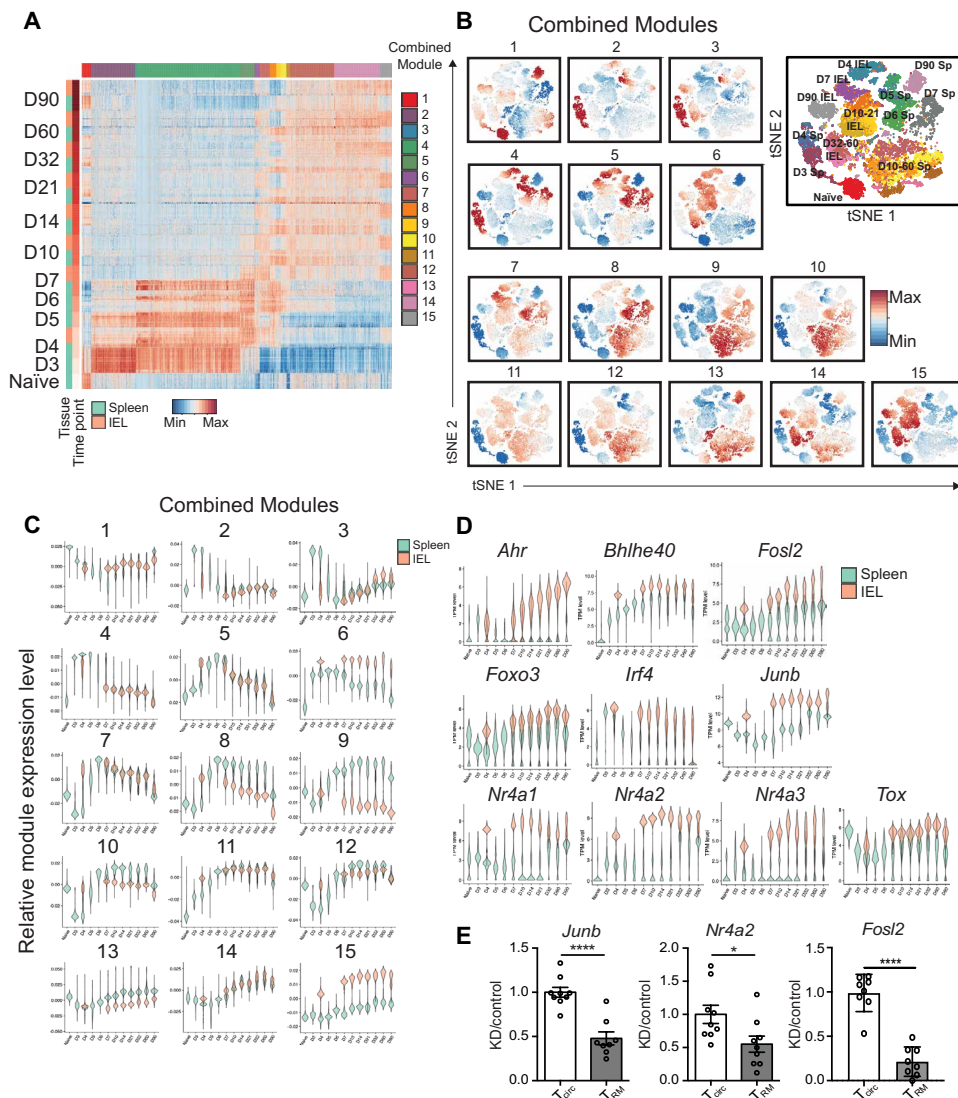
Fig. 2. Identification of a siIEL CD8+ T cell–enriched gene expression profile. (**A**) Gene expression patterns of single splenic and siIEL CD8+ T cells responding to infection, where each row represents an individual cell, grouped by tissue within each time point, and each column represents an individual gene, grouped by module, represented as expression relative to the mean expression among all cells. Weighted gene coexpression network analyses of splenic and siIEL CD8+ T cells considered together were performed to derive gene modules. (**B** and **C**) Representation of each module among single CD8+ T cells in both the spleen and siIEL compartment over time, relative to the mean representation among all cells, depicted as a representation score superimposed on individual cells (B) or as violin plots showing the relative representation of each module in individual splenic (teal) versus siIEL CD8+ T cells (coral) (C). (**D**) Violin plots depicting gene expression patterns of known or putative regulators of T_{RM} cell differentiation [represented as transcripts per million (TPM)], selected from siIEL CD8+ T cell–enriched modules, among single splenic (teal) or siIEL (coral) CD8+ T cells over time. (**E**) CD45.1+ P14 T cells were transduced with retrovirus encoding shRNA targeting $Nr4a2$, $Junb$, or $Fosl2$ (KD) and mixed with CD45.1.2+ P14 T cells transduced with shRNA encoding control (nontarget) shRNA at a 1:1 ratio of KD/control cells before adoptive transfer into CD45.2+ hosts that were subsequently infected with LCMV. Twenty-two to 26 days later, splenic and siIEL CD8+ T cells were analyzed by flow cytometry. Ratio of KD/control P14 T cells within transduced P14 CD8+ T cells in the spleen (T_{circ}) or within CD69+CD103+ siIEL P14 CD8+ T cells (T_{RM}), normalized to the ratio of KD/control cells at the time of transfer. Values are normalized to T_{circ}. *$P < 0.05$ and ****$P < 0.0001$ (Student's two-tailed t test). Data were pooled from two independent experiments, with means and SEM of $n = 8$ mice per gene, where each circle represents an individual mouse.

undergoing differentiation and demonstrate the potential value of this dataset in identifying previously unknown genes and pathways involved in specifying T_{RM} cell versus circulating memory CD8+ T cell fates.

scRNA-seq analyses highlight circulating CD8+ T cell heterogeneity and reveal previously unappreciated heterogeneity within the siIEL CD8+ T cell pool

We next investigated potential heterogeneity of differentiating splenic and siIEL CD8+ T cells. We observed that individual splenic CD8+ T cells at certain time points expressed genes previously associated with CD8+ T cell subsets, such as terminal effector (TE) and memory precursor (MP) phenotype cells at the peak of infection, and T_{EM}, T_{CM}, and LLE cell subsets at later time points after infection (Fig. 3, A and B). For example, the majority of cells at days 6 and 7 after infection expressed high levels of $Klrg1$, likely representing TE cells, whereas a smaller number of cells exhibited lower expression of $Klrg1$ and higher expression of $Tcf7$ and $Bcl2$, likely representing MP cells (48–50). We also observed that certain cells at later time points expressed genes previously associated with T_{CM} ($Il7r$, $Tcf7$, $Sell$, $Bcl2$, and $Cxcr3$), LLE ($Klrg1$, $Cx3cr1$, and $Zeb2$), and T_{EM} (intermediate levels of $Cx3cr1$, $Zeb2$, $Il7r$, $Tcf7$, and $Bcl2$) cells (Fig. 3, A and B) (1, 3). Mapping individual splenic CD8+ T cells to TE, MP, T_{CM}, T_{EM}, and LLE transcriptional signatures defined by bulk RNA-seq signatures of sorted cells from each subset revealed that heterogeneity observed among splenic CD8+ T cells might represent cells differentiating into each of these memory cell subsets (Fig. 3, C and D). Low, intermediate, or high expression of $Cx3cr1$ at day 6 after infection generally corresponded to cells with T_{CM}, T_{EM}, or LLE profiles, respectively, consistent with previously reported CX3CR1^{hi}, CX3CR1^{int}, and CX3CR1^{lo} subsets with distinct functional capacities and terminal differentiation potentials that can be found at the peak of infection (Fig. 3, B and D) (51). These results demonstrate the concurrent presence of these memory subsets within the circulating CD8+ T cell memory pool, consistent with previous studies (4–6, 52), and support findings suggesting that these memory
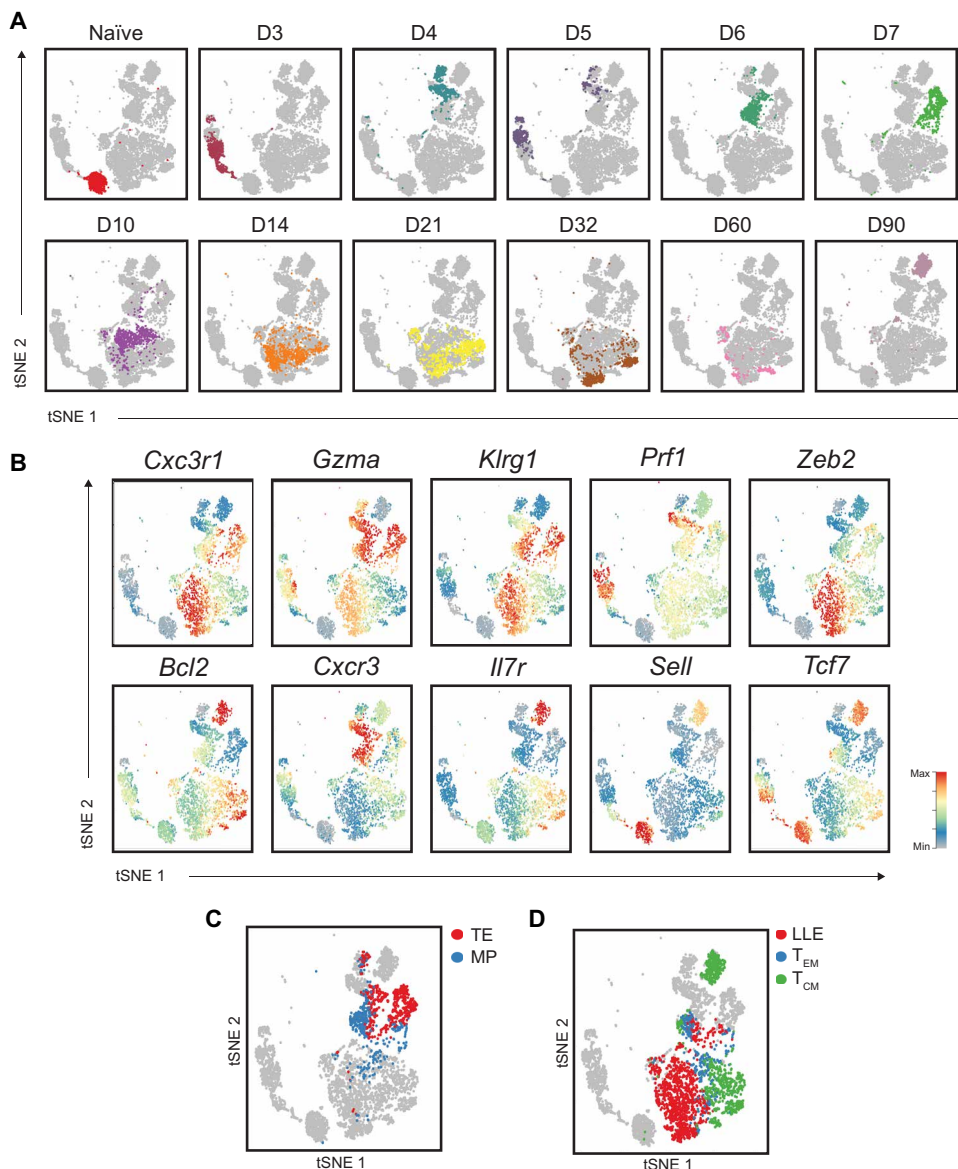
reduction in siIEL T_{RM} cells than splenic memory CD8+ T cells (Fig. 2E and fig. S6B). Together, these results highlight key transcriptional differences between circulating and siIEL CD8+ T cells

Fig. 3. scRNA-seq analyses highlight heterogeneity among circulating CD8+ T cells. (**A**) tSNE analysis of splenic CD8+ T cells; each plot represents an individual time point with each color representing a specific time point, as in Fig. 1B. (**B**) Relative expression (compared with mean expression among all spleen cells) of known regulators of circulating CD8+ T cell differentiation superimposed on individual spleen cells. (**C** and **D**) Similarity of gene expression programs among single spleen cells to transcriptional signatures (derived from bulk RNA-seq profiles from FACS-sorted cells) of previously defined circulating CD8+ T cell subsets. (C) Similarity of gene expression programs among single spleen cells to TE (D7 KLRG1hiIL-7Rαlo; red) or MP (D7 KLRG1loIL-7Rαhi; blue) transcriptional signatures. (D) Similarity of gene expression programs among single spleen cells to LLE (D35 CD62LloIL-7Rαlo; red), T_{EM} (D35 CD62LloIL-7Rαhi; blue), and T_{CM} (D35 CD62LhiIL-7Rαhi; green) cell transcriptional signatures.

CD8+ T cell subsets may begin to diverge in their differentiation pathways earlier than is widely appreciated (*51*). These analyses also uncovered a notable transcriptional divergence between cells at days 60 versus 90 after infection (Fig. 3A). Prior studies have shown that T_{CM} cells are the predominant circulating memory subset at late time points, but whether and how T_{CM} cells change transcriptionally at late time points has not been investigated in depth. Compared with day 60 T_{CM} cells, day 90 T_{CM} cells expressed higher levels of *Eomes* and lower levels of genes encoding cytolytic granules such

as *Gzma* and *Gzmb*, suggesting a progressive loss of cytotoxic capability over time (table S4). Moreover, these analyses highlighted a number of genes without known functions in T_{CM} cell differentiation and/or maintenance, such as *Hspa1a* and *Hspa1b*, which encode members of a family of conserved heat shock proteins (HSP70) that plays a role in protecting against cellular stressors, including hypoxia, temperature aberrations, pH alterations, and oxidative stress (*53*).

Although heterogeneity within circulating CD8+ T cells has been relatively well described, whether heterogeneity exists within tissue-resident CD8+ T cell populations remains unclear. To investigate potential heterogeneity within the siIEL CD8+ T cell compartment, we defined cell clusters across the entire dataset, revealing 40 distinct clusters, 17 of which were found in the siIEL compartment (Fig. 4A). We also performed partition-based graph abstraction (PAGA) trajectory analysis (*54*) to infer relationships between the siIEL clusters we defined (fig. S7). We observed that multiple clusters of siIEL CD8+ T cells were present within several individual time points, suggesting that distinct subsets might exist within the siIEL CD8+ T cell population (Fig. 4B). For example, at day 60 after infection, two major cell clusters, Clusters 3 and 29, were observed. These clusters exhibited differential expression of 236 genes, including several transcription factors, suggesting that these clusters were regulated by distinct gene expression programs (table S5). For example, Cluster 3 cells had higher expression of *Id3*, *Jun*, *Fos*, *Klf2*, and *Myc*, whereas Cluster 29 cells had higher expression of transcription factors including *Bcl6*, *Zeb2*, and *Klf3*. Cluster 3 cells also exhibited higher expression of several genes associated with T_{RM} cell function, including cytokines and chemokines (*Ifng*, *Tnf*, *Ccl3*, and *Ccl4*), suggesting that Cluster 3 cells might be better poised to produce cytokines rap-

idly upon reinfection (Fig. 4C and table S5). Cluster 3 cells also had higher transcript levels of the transcription factor Id3, and a recent study identified an Id3hi T_{RM} cell subset with distinct functional capabilities including an enhanced capacity to produce cytokines (*55*). These analyses suggest that distinct costimulatory and other signaling pathways might be responsible for regulating each of these cell clusters and raised the possibility that these cell clusters might have distinct functional capacities. Consistent with this possibility, PAGA analysis revealed that whereas Cluster 3 cells were linked to

Fig. 4. scRNA-seq analyses reveal functionally distinct subsets within the siIEL CD8⁺ T cell pool. (**A** and **B**) Clustering analyses of siIEL CD8⁺ T cells from all time points (A) or cells at days 4, 60, and 90 after infection (B); numbers represent different cluster annotations. (**C** and **D**) Expression of selected genes within single siIEL CD8⁺ T cells at day 60 (C) or day 90 (D) after infection, relative to the mean expression among siIEL CD8⁺ T cells at the indicated time point, demonstrating differential gene expression between Clusters 3 and 29 (C) or between Clusters 17 and 19 (D). (**E** to **I**) P14 CD8⁺ T cells were transferred into congenically distinct recipients 1 day before infection with LCMV. Splenic and siIEL CD8⁺ T cells were harvested at day 30 or 90 after infection. (E) Representative flow cytometry plots displaying distribution of CD28 expression among total P14 T cells in the spleen (top) or CD69⁺CD103⁺ P14 T cells in the siIEL compartment (bottom). Numbers represent the percentage of total P14 T cells in each gate, and graphs to the right demonstrate the quantification of CD28^{lo} (filled circles) and CD28^{hi} (open circles) cells within the indicated population at each time point. Data are representative of (flow cytometry plots; left) or compiled from (graphs; right) three independent experiments where $n = 2$ to 5 mice per experiment (10 to 11 total mice). (F) Quantification of CD127 (IL-7Rα) expression by CD28^{lo} (gray) or CD28^{hi} (black) subsets within the spleen (top) or siIEL (bottom) at day 30 after infection, with representative flow cytometry plots shown on the left. Numbers represent mean fluorescence intensity (MFI) of CD127 within the indicated population. Data are representative of (left) or compiled from (graph on right side) $n = 3$ independent experiments with $n = 7$ total mice, where each circle represents an individual mouse. (G) Representative flow cytometry plots displaying (top) distribution of CD28 expression at day 30 after infection among total H-2D^b GP$_{33-41}$ tetramer⁺ endogenous CD8⁺ T cells in the spleen (left) or among H-2D^b GP$_{33-41}$ tetramer⁺ endogenous CD69⁺CD103⁺ CD8⁺ T cells in the siIEL compartment (right) or displaying (bottom) expression of CD127 by CD28^{lo} (gray) or CD28^{hi} (black) subsets within the indicated compartment. Numbers represent the percentage of H-2D^b GP$_{33-41}$ tetramer⁺ cells in each gate (top) or MFI of CD127 expression in the indicated population (bottom), quantified in the graph (right), where $n = 4$ individual mice. (H and I) At day 30 after infection, siIEL P14 T cells were sorted into CD127^{lo} and CD127^{hi} subsets and cultured in the presence of GP$_{33-41}$ peptide in vitro. Quantification (right) of the proportion of CD127^{hi} or CD127^{lo} P14 siIEL CD8⁺ T cells producing IFN-γ and TNF-α (H) or IL-2 and TNF-α (I) as shown in

representative flow cytometry plots (left). Data are representative of two independent experiments, with means and SEM of $n = 4$ wells of cultured cells per phenotype, derived from two separate pools of sorted cells plated in duplicate. *$P < 0.05$, **$P < 0.01$, and ****$P < 0.0001$ [paired t test (F and G) or Student's two-tailed t test (H and I)].
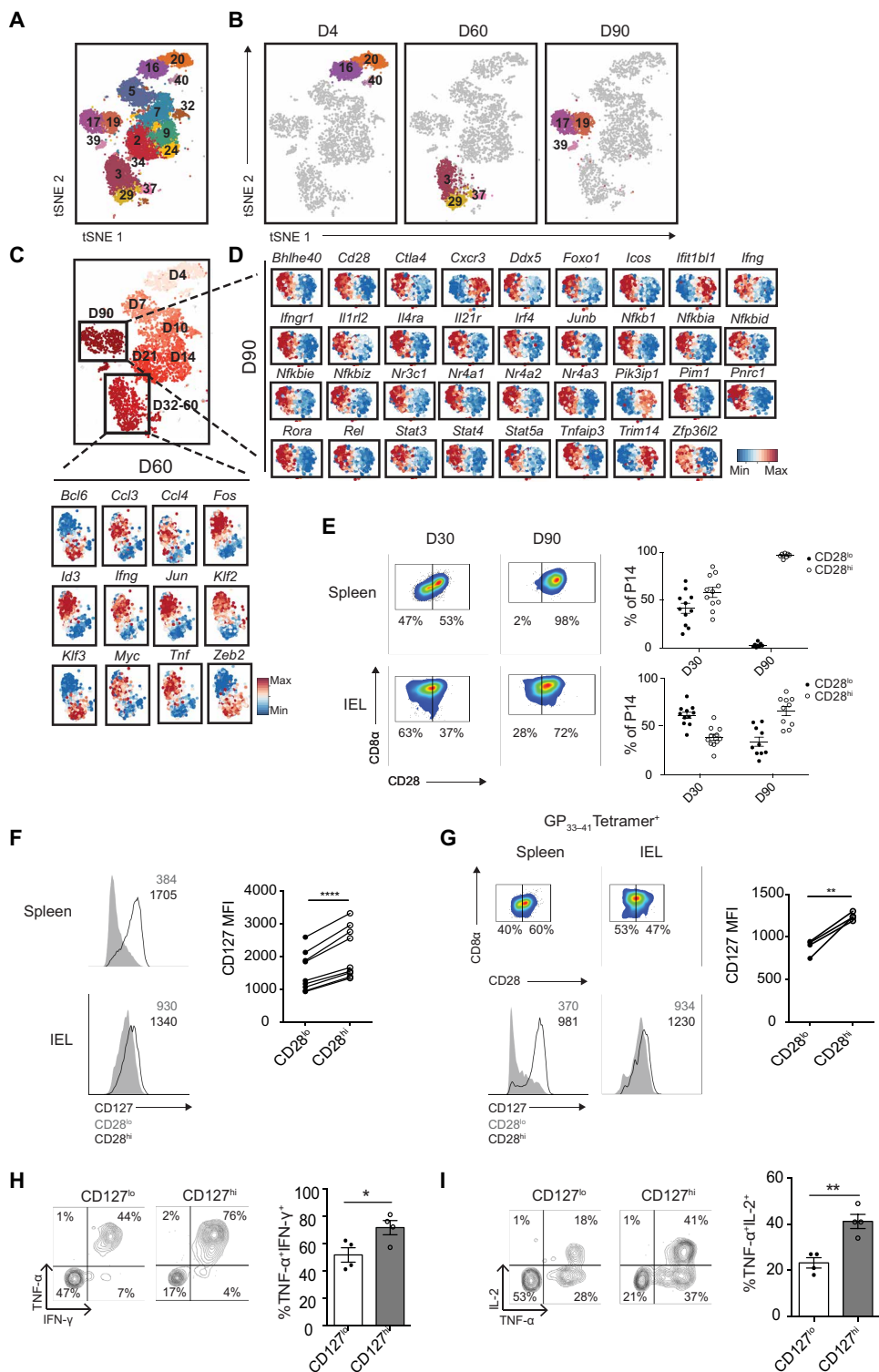
day 90 clusters, Cluster 29 cells were not, suggesting that Cluster 29 cells might represent a terminal state (fig. S7). These findings are consistent with increased expression of the transcription factor

Zeb2, which is known to promote the terminal differentiation of circulating CD8⁺ T cells (*33*), by Cluster 29, and the reciprocal increased expression among Cluster 3 cells of the transcription

factor *Id3*, which is known to regulate the development of long-lived circulating memory CD8$^+$ T cells (*56, 57*).

In addition, at day 90 after infection, two major cell clusters, Clusters 17 and 19, were observed; these clusters exhibited differential expression of 361 genes (table S6). Cluster 17 cells exhibited higher expression of 243 genes, including transcription factors (*Bhlhe40, Ddx5, Foxo1, Irf4, Junb, Nr3c1, Nr4a1, Nr4a2, Nr4a3, Pnrc1,* and *Rora*) and mediators of cytokine signaling (*Ifngr1, Il1rl2, Il21r, Il4ra, Stat3, Stat5a,* and *Stat4*). Cluster 17 cells also exhibited higher expression of *Zfp36l2*, which encodes for a zinc finger protein involved in the regulation of mRNA decay (*58*), and the transcript for interferon-γ (IFN-γ), as well as genes associated with pathways that were highly represented within T$_{RM}$ cell–enriched modules, such as the regulation of NF-κB signaling (*Nfkbia, Nfkbid, Tnfaip3, Pim1, Rel, Nfkb1, Nfkbie,* and *Nfkbiz*) and costimulatory and inhibitory molecules *Icos* and *Ctla4* (Fig. 4D and table S6). Cluster 17 cells also exhibited higher expression of the costimulatory receptor *Cd28*, suggesting that costimulation through this receptor could specifically influence the differentiation or responsiveness of a specific subset of T$_{RM}$ cells. By contrast, Cluster 19 exhibited higher expression of 117 genes, including the tissue-homing molecule *Cxcr3*, interferon response genes (*Trim14* and *Ifit1bl1*), and *Pik3ip1*, a negative regulator of T cell activation (Fig. 4D and table S6). Together, these findings suggested that specific cytokine and/or costimulatory signals might be responsible for maintaining or directing the differentiation of Cluster 17 cells. Moreover, whereas Cluster 17 cells might be better poised to produce cytokines rapidly upon reinfection, Cluster 19 cells might be more likely to respond immediately to type I interferon signals within the tissue. These data suggest that multiple subsets with distinct transcriptional programs and functional capacities may exist within the T$_{RM}$ cell pool.

We next performed flow cytometry to determine whether the heterogeneity revealed by scRNA-seq analyses could be discerned at the protein level. CD45.1$^+$ P14 CD8$^+$ T cells were adoptively transferred into congenic CD45.2$^+$ hosts that were infected with LCMV 1 day later. At days 30 and 90 after infection, the spleens and siIEL compartments of recipient mice were harvested for analysis. At day 30 after infection, both splenic and siIEL CD8$^+$ T cells could be divided into CD28^{hi} and CD28^{lo} populations (Fig. 4E). In contrast, at day 90 after infection, splenic P14 CD8$^+$ T cells uniformly expressed high levels of CD28, but heterogeneity was retained within the siIEL P14 CD8$^+$ T cell population (Fig. 4E), in line with data revealing multiple clusters within the T$_{RM}$ cell population with differential expression of *Cd28* at the mRNA level at day 90 after infection (Fig. 4D). We also noted that high expression of IL-7Rα (CD127), which was observed in the functionally distinct Id3^{hi} T$_{RM}$ cell subset described in a recent study (*55*), also correlated with high expression of CD28 (Fig. 4F). We also observed this heterogeneity among endogenous, siIEL CD8$^+$ H-2D^b GP$_{33–41}$ tetramer$^+$ cells, with CD28^{hi} cells expressing higher levels of CD127 (Fig. 4G). To investigate whether heterogeneity in expression of these markers might reflect functional heterogeneity, we sorted CD127^{hi} and CD127^{lo} populations from the siIEL CD8$^+$ T cell pool at day 30 after infection and measured their capacities to produce cytokines when rechallenged with cognate antigen in vitro. We found that CD127^{hi} cells produced higher levels of the cytokines IFN-γ, tumor necrosis factor–α (TNF-α), and IL-2 in response to restimulation than did CD127^{lo} cells (Fig. 4, H and I), consistent with enhanced cytokine production in Id3^{hi} T$_{RM}$ cells (*55*), and the higher level of *Ifng* tran-

script detected within CD28^{hi} cells at day 90 after infection (Fig. 4, C and D). Although it remains possible that differences in the ability to produce cytokine upon restimulation may reflect different responses to ex vivo conditions, the observation that these two populations respond differently suggests that they are functionally distinct. Together, these data demonstrate that the heterogeneity revealed by scRNA-seq analyses within the T$_{RM}$ cell pool at late time points after infection may be functionally important.

The observation that expression of a number of transcriptional regulators, including *Ddx5, Junb, Nr4a2,* and *Pnrc1,* as well as the RNA binding protein *Zfp36l2,* correlated with *Cd28* expression (Fig. 4D), raised the possibility that these genes might represent regulators of T$_{RM}$ cell heterogeneity. To investigate this possibility, we transduced P14 CD8$^+$CD45.1$^+$ T cells with retroviruses encoding shRNA targeting *Junb, Nr4a2, Pnrc1,* or *Zfp36l2* before adoptive transfer into congenic CD45.2$^+$ hosts that were subsequently infected with LCMV. Knockdown of *Nr4a2* and *Junb* resulted in a loss of total T$_{RM}$ cells, whereas knockdown of *Pnrc1* or *Zfp36l2* did not affect the size of the total T$_{RM}$ cell population (fig. S6C). However, knockdown of each of these genes resulted in a reduction in the proportion of siIEL T$_{RM}$ (CD69$^+$CD103$^+$) cells expressing high levels of CD28 compared with congenically distinct, cotransferred control P14 CD8$^+$ T cells transduced with retroviruses encoding nontargeting shRNA (Fig. 5A and fig. S6C). In addition, we cotransferred P14 CD8$^+$ T cells from mice with a T cell–specific deletion of *Ddx5* (*Ddx5$^{fl/fl}$*CD4cre$^+$: "*Ddx5$^{-/-}$*") and congenically distinct control P14 CD8$^+$ T cells (*Ddx5$^{fl/fl}$*CD4cre$^-$: "WT") into recipients infected with LCMV 1 day later and found that although *Ddx5* deletion resulted in a severe depletion of both the total circulating memory T cell and total T$_{RM}$ cell populations, the proportion of CD28^{hi} cells was further reduced among the remaining *Ddx5$^{-/-}$* T$_{RM}$ cell population (Fig. 5B and fig. S6C). Moreover, consistent with this decrease in the proportion of CD28^{hi} cells, *Ddx5$^{-/-}$* siIEL, but not splenic, CD8$^+$ T cells exhibited a reduced ability to produce IFN-γ and TNF-α upon restimulation with cognate antigen in vitro (Fig. 5C). Together, these findings suggest that, similar to *Prdm1* and *Id3* (*55*), *Ddx5, Junb, Nr4a2, Pnrc1,* and *Zfp36l2* regulate the differentiation of transcriptionally and functionally distinct T$_{RM}$ cell subsets.

Although it is known that two distinct populations with differing memory potentials, distinguished by high or low expression of the high-affinity IL-2 receptor, IL-2Rα (CD25) (*59, 60*), exist within the circulating CD8$^+$ T cell pool early in infection, whether the CD8$^+$ T cell pool that seeds the tissue early in infection is heterogeneous remained unknown. To determine whether heterogeneity of siIEL CD8$^+$ T cells can be discerned early after infection, we next examined the earliest time point, day 4 after infection, at which CD8$^+$ T cells could be detected in the siIEL compartment. In addition to the heterogeneity observed at late time points after infection (Fig. 4B), two major clusters, Clusters 16 and 20, were evident at day 4 after infection and exhibited differential expression of 332 genes (Figs. 4B, 5B, and 6A and table S7). Only 17 of these genes were more highly expressed by Cluster 16 cells, such as interferon response genes *Ifit1, Ifit1bl1,* and *Ifit3; Pik3ip1,* a negative regulator of TCR signaling; *Mxd4,* a Myc-antagonist that promotes survival in T cells (*61*); and *Kdm5b,* a histone demethylase (Fig. 6A and table S7). GO analyses revealed that the genes expressed more highly by Cluster 20 cells were overrepresented in biologic processes such as DNA replication, mitotic spindle and nucleosome assembly, cytokinesis, and cell division; specific genes included *Cdc7, Cdc25b, Cenpk,*
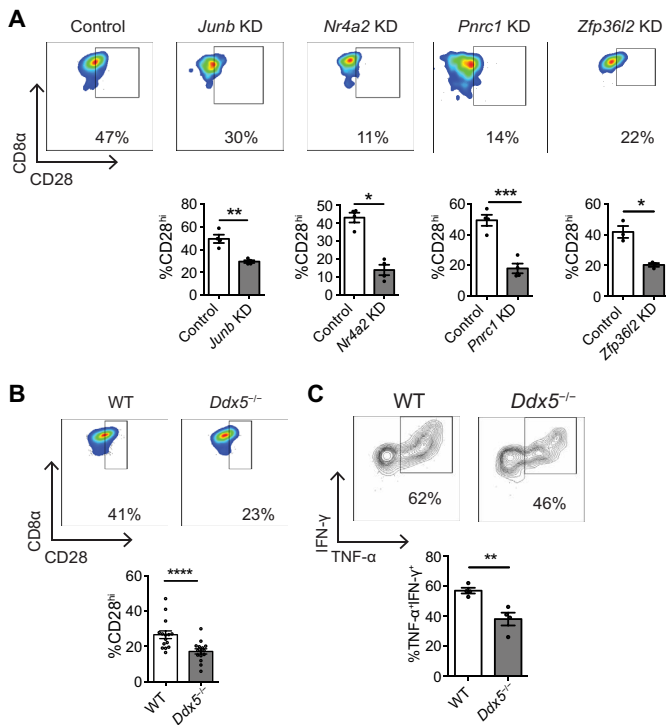
Fig. 5. scRNA-seq analyses identify putative regulators of CD8$^+$ T$_{RM}$ cell heterogeneity. (**A**) CD45.1$^+$ P14 T cells were transduced with retrovirus encoding shRNA targeting the indicated genes (KD) and mixed with CD45.1.2$^+$ P14 T cells transduced with shRNA encoding control (nontarget) shRNA at a 1:1 ratio of KD/control cells before adoptive transfer into CD45.2$^+$ hosts that were subsequently infected with LCMV, as in fig. S6. Twenty-two to 23 days later, siIEL CD8$^+$ T cells were analyzed by flow cytometry. Quantification of the percentage of nontarget or KD P14 CD8$^+$ T$_{RM}$ cells (CD69$^+$CD103$^+$) expressing high levels of CD28 (bottom) as shown in representative flow cytometry plots (top). Data are representative of one to two experiments, with means and SEM of $n = 4$ mice per gene, where each circle represents an individual mouse. (**B** and **C**) P14 CD8$^+$ T cells from mice with T cell–specific deletion of *Ddx5* (*Ddx5*$^{fl/fl}$ CD4-Cre$^+$: *Ddx5*$^{-/-}$) were cotransferred at a 1:1 ratio with congenically distinct control P14 CD8$^+$ T cells (*Ddx5*$^{fl/fl}$ CD4-Cre$^-$: WT) into congenically distinct hosts that were infected with LCMV 1 day later. At day 30 after infection, spleens and siIEL were harvested for flow cytometric analysis. (B) Quantification of the percentage of *Ddx5*$^{-/-}$ or WT P14 CD8$^+$ T$_{RM}$ cells (CD69$^+$CD103$^+$) expressing high levels of CD28 (bottom) as shown in representative flow cytometry plots (top). (C) Lymphocytes harvested from siIEL compartment were cultured in the presence of GP$_{33-41}$ peptide in vitro before staining for flow cytometric analysis. Cytokine production in *Ddx5*$^{-/-}$ or WT siIEL P14 CD8$^+$ T cells, shown as quantification of the proportion of cells producing TNF-α and IFN-γ (bottom), as shown in representative flow cytometry plots (top). Data are compiled from (B) or representative of (C) two independent experiments with means and SEM of $n = 4$ to 12 mice, where each circle represents an individual mouse. *$P < 0.05$, **$P < 0.01$, ***$P < 0.001$, and ****$P < 0.0001$ (paired t test).

Cenpm, *Cdc20*, and *Cdk1* (Fig. 6A and table S7). Moreover, additional analyses confirmed that a greater proportion of Cluster 20 cells were in the G$_2$-M phases of the cell cycle compared with Cluster 16 cells, indicating that cells in Cluster 20 were more actively proliferating (Fig. 6B). Cluster 20 cells also expressed higher levels of *Dnmt1*, a DNA methyltransferase that is critical for the expansion of CD8$^+$ T cells during the effector phase of the immune response (*62*), along with several components of the polycomb repressive complex 2, including *Suz12* and *Ezh2* (Fig. 6A), which negatively regulates gene expression via histone methylation and has been

previously shown to promote effector CD8$^+$ T cell differentiation by mediating the repression of memory-associated genes (*20*, *63*). Consistent with these findings, PAGA trajectory analysis (fig. S7) revealed that whereas Cluster 16 cells were linked to day 7 clusters, Cluster 20 cells were not, suggesting that Cluster 20 cells might be undergoing terminal differentiation, whereas Cluster 16 cells might represent precursors to siIEL CD8$^+$ T$_{RM}$ cells.

To formally test this possibility, we adoptively transferred P14 CD8$^+$CD45.1$^+$ T cells into CD45.2$^+$ hosts infected with LCMV 1 day later and harvested the siIEL compartment at day 4 after infection for flow cytometric analysis. We found that, in addition to IL-2Rα^{hi} and IL-2Rα^{lo} subsets within the early circulating CD8$^+$ T cell population, there was also heterogeneity in IL-2Rα expression among day 4 CD8$^+$ T cells within the small intestinal epithelial tissue; this heterogeneity was also evident among endogenous siIEL CD8$^+$ H-2D^b GP$_{33-41}$ tetramer$^+$ cells at day 4 after infection (Fig. 6C). We also found that protein expression of IL-2Rα and Ezh2 was correlated (Fig. 6D) and took advantage of this observation to test whether these populations within the tissue have distinct differentiation potentials. CD45.1$^+$ CD8$^+$IL-2Rα^{hi} or CD8$^+$IL-2Rα^{lo} cells from the siIEL compartment were FACS-sorted at 4 days after infection and adoptively transferred intravenously into CD45.2$^+$ recipient mice infected with LCMV 1 day before transfer; analysis of siIEL CD8$^+$ T cells was performed 7 or 30 days later (Fig. 6E). P14 CD8$^+$ T cells within the siIEL compartment of mice that had received IL-2Rα^{lo} cells expressed lower levels of KLRG1 at day 7 after infection (Fig. 6F), indicating a less terminally differentiated phenotype. Moreover, mice that had received IL-2Rα^{lo} P14 siIEL CD8$^+$ cells had a higher proportion of CD69$^+$CD103$^+$ P14 CD8$^+$ T cells within the siIEL compartment at both days 7 and 30 (Fig. 6G), suggesting that IL-2Rα^{lo} siIEL CD8$^+$ T cells at day 4 after infection are more likely to give rise to bona fide T$_{RM}$ cells that persist long-term. Together, these data suggest that, analogous to IL-2Rα^{lo} and IL-2Rα^{hi} populations within the circulating CD8$^+$ T cell pool early in infection (*59*, *60*), two functionally distinct CD8$^+$ T cell populations are present within the siIEL compartment at day 4 after infection: a IL-2Rα^{hi} subset with a more terminally differentiated phenotype that likely represents a transient tissue effector population and a IL-2Rα^{lo} subset with higher memory potential that likely contains the precursors of T$_{RM}$ cells. Cluster 20 cells, corresponding to the IL-2Rα^{hi} population, are more proliferative, exhibit a transcriptional profile that includes factors that are associated with the effector CD8$^+$ T cell fate (*Ezh2* and *Dnmt1*), and are more likely to give rise to terminally differentiated effector-like CD8$^+$ T cells. In contrast, Cluster 16 cells, corresponding to the IL-2Rα^{lo} subset, may be more quiescent and better poised to respond to type I interferons, have greater survival capacity, and have greater potential to give rise to long-lived T$_{RM}$ CD8$^+$ T cells. Together, these results demonstrate previously unappreciated transcriptional and functional heterogeneity within the siIEL CD8$^+$ T cell pool at multiple states of differentiation.

DISCUSSION

Recent studies have begun to elucidate key regulators of T$_{RM}$ cell differentiation, function, and survival, such as the transcription factors Blimp1, Hobit, and Runx3. Our scRNA-seq analyses have identified a number of additional putative regulators of T$_{RM}$ cell differentiation. For example, *Nr4a2*, *Junb*, and *Fosl2* were among the 528 genes that were substantially enriched in siIEL CD8$^+$ T cells relative to
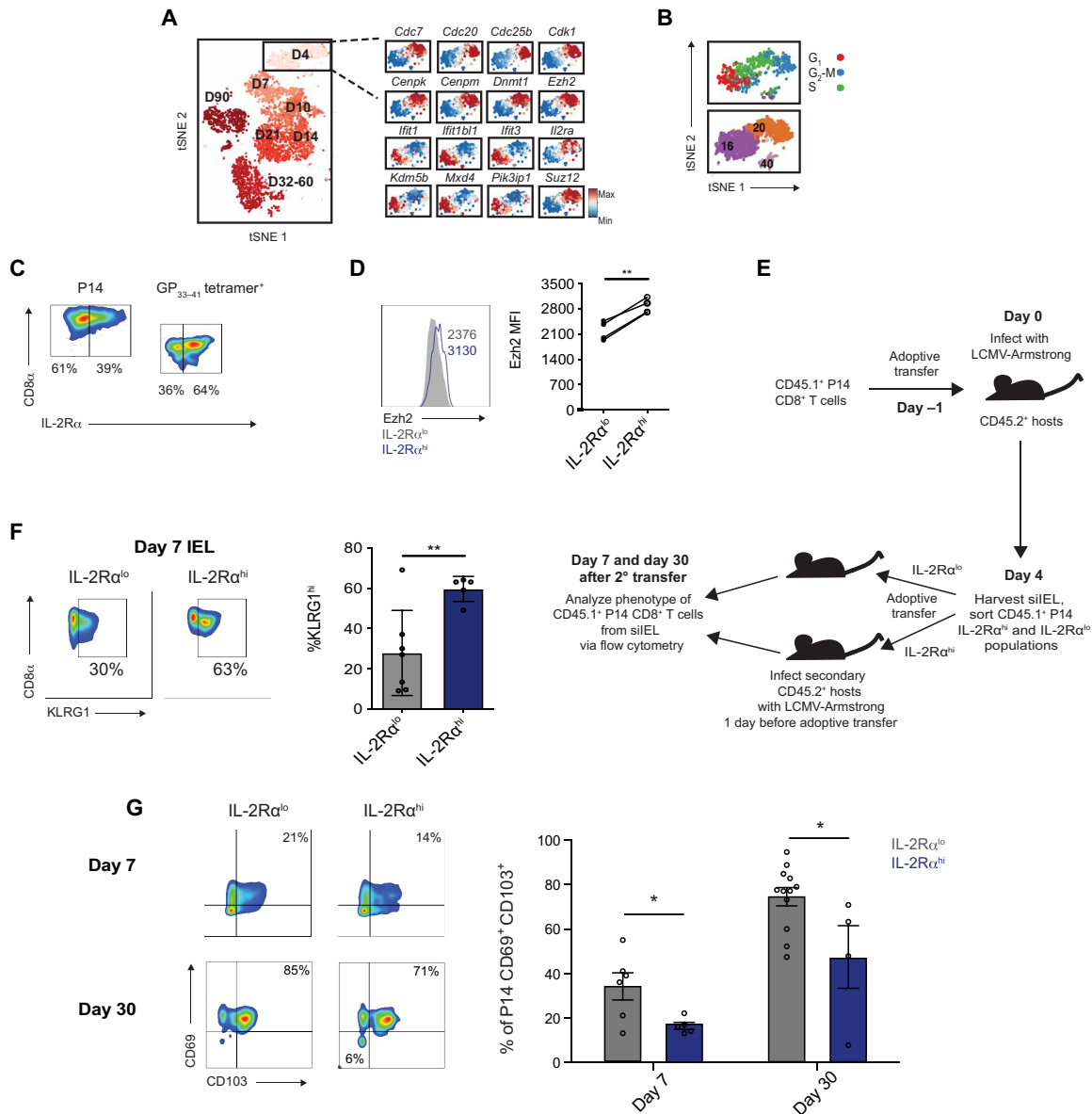
Fig. 6. T_RM cell precursors identified within the siIEL CD8+ T cell pool early in infection. (**A**) Expression of selected genes within single siIEL CD8+ T cells at day 4 after infection, relative to the mean expression among all cells, demonstrating differential gene expression between cells in Clusters 16 and 20. (**B**) Cell cycle status of siIEL CD8+ T cells at day 4 after infection, inferred from transcriptional profiles. (**C** and **D**) P14 CD8+ T cells were adoptively transferred into congenic hosts 1 day before infection with LCMV. Splenic and siIEL CD8+ T cells were analyzed by flow cytometry at day 4 after infection. Data are representative of two independent experiments, with $n = 2$ to 3 mice per experiment. (C) Representative flow cytometry plots displaying distribution of IL-2Rα expression among total siIEL P14 CD8+ T cells at day 4 after infection (left) or among total H-2D^b GP_{33–41} tetramer+ endogenous siIEL CD8+ T cells at day 4 after infection in mice that had not received adoptive transfer of P14 CD8+ T cells (right). (D) Quantification of Ezh2 expression among IL-2Rα^lo (gray) and IL-2Rα^hi (blue) P14 siIEL CD8+ T cells, as gated in (C), with representative flow cytometry plot (left) and quantification (right). Numbers represent MFI of Ezh2 within the indicated population. Data are representative of (plot to left) or compiled from (graph to right) two independent experiments, with $n = 4$ total mice, where each dot represents an individual mouse. (**E**) Schematic of experimental setup. CD45.1+ P14 CD8+ T cells were adoptively transferred into CD45.2+ congenic hosts 1 day before infection with LCMV. CD45.1+ P14 CD8+ T cells were collected from the siIEL compartment at day 4 after infection and sorted on the basis of expression of IL-2Rα as shown in (C). IL-2Rα^hi and IL-2Rα^lo populations were adoptively transferred into secondary hosts that had been infected with LCMV 1 day before transfer. Seven or 30 days later, siIEL P14 CD8+ T cells were analyzed by flow cytometry. (**F**) Quantification of the proportion of KLRG^hi P14 CD8+ T cells present within the siIEL compartment at day 7 after infection. Data were pooled from two independent experiments, with means and SEM of $n = 7$ (IL-2Rα^lo) or 5 (IL-2Rα^hi), where each circle represents an individual mouse. (**G**) Quantification of the percentage of siIEL CD45.1+ P14 CD8+ CD69+CD103+ T cells derived from IL-2Rα^lo (gray) or IL-2Rα^hi (blue) day 4 siIEL cells at day 7 or day 30 after transfer, with representative flow cytometry plots shown to the left. Day 7 data were pooled from two independent experiments, with means and SEM of $n = 5$ (IL-2Rα^hi) or 6 (IL-2Rα^lo) hosts, where each circle represents an individual mouse. Day 30 data were pooled from three independent experiments, with means and SEM of $n = 4$ (IL-2Rα^hi) or 12 (IL-2Rα^lo) hosts, where each circle represents an individual mouse. *$P < 0.05$ and **$P < 0.01$ [paired t test (D) or Student's two-tailed t test (F and G)].

splenic cells at all time points after infection, and we found that knockdown of *Nr4a2*, *Junb*, or *Fosl2* resulted in impaired T_{RM} cell differentiation. *Junb* and *Fosl2* encode for AP-1 dimerization partners that have been reported to repress T-bet expression in T_H17 cells (46, 47). Given that down-regulation of T-bet expression is important for early establishment of the T_{RM} cell transcriptional program (15), it is tempting to speculate that *Junb* and *Fosl2* may regulate T_{RM} cell differentiation by cooperatively regulating T-bet expression. Because *Fosl2* has been previously reported to positively regulate *Smad3* (47), a key component of the TGF-β signaling pathway, *Fosl2* may also promote T_{RM} cell differentiation through effects on TGF-β signaling.

In addition to identifying specific putative regulators of T_{RM} cell differentiation, our analyses have implicated new pathways that may control aspects of T_{RM} cell biology. For example, we observed that siIEL CD8$^+$ T cells exhibited increased levels of transcripts associated with TCR signaling, even after infection had been cleared and antigen was no longer present, suggesting that CD8$^+$ T cells within tissues are transcriptionally poised for rapid responsiveness to TCR stimulation. Because T_{RM} cells have been reported to exhibit a decreased ability to scan for antigens owing to reduced motility relative to circulating CD8$^+$ T cells (64, 65), such enhanced TCR responsiveness might represent a potential mechanism enabling T_{RM} cells to mount robust protective responses even in the face of limiting amounts of cognate antigen. Moreover, we observed that differentiating siIEL CD8$^+$ T cells also exhibited sustained expression of genes encoding inhibitory receptors, including *Ctla4*, *Tigit*, and *Lag3*, consistent with prior reports (13, 18), which may provide a balance against higher basal TCR responsiveness and enable T_{RM} cells to avoid excessive responses that might lead to autoimmune pathology (66).

Our analyses also provide new insights regarding T_{RM} cell ontogeny, which has not been as well studied as that of circulating memory CD8$^+$ T cells (20, 59, 67). Other than the observations that T_{RM} cells are derived from circulating cells lacking high expression of KLRG1 (13, 16) and share a common clonal origin as T_{CM} cells (68), very little is known about the precursors of T_{RM} cells after their arrival in the tissue. We found that siIEL CD8$^+$ T cells were transcriptionally distinct from splenic CD8$^+$ T cells at 4 days after infection, the earliest time point at which these cells can be detected within the small intestinal tissue (30). One interpretation of this finding is that transcriptional changes induced by the local tissue microenvironment occur rapidly upon tissue entry. Alternatively, CD8$^+$ T cells that seed tissues may represent precommitted T_{RM} cell precursors that have already acquired some aspects of the T_{RM} cell transcriptional program. Although there were distinct clusters of splenic CD8$^+$ T cells observed at day 3 after infection, none of these clusters appeared to be transcriptionally similar to siIEL CD8$^+$ T cells. This finding suggests that the T_{RM} cell transcriptional program may not be initiated until after the cells have entered the tissue and does not support the hypothesis that precommitted T_{RM} precursor cells are formed within the circulating CD8$^+$ T cell pool. However, it has been previously shown that priming by DNGR-1$^+$ dendritic cells in the draining lymph nodes is an important step for T_{RM} cell differentiation in vaccinia virus infection in the skin and influenza A infection in the lung (69). These findings suggest that the mechanisms underlying early T_{RM} cell fate specification might differ for localized infections and might even be distinct among different tissues or pathogens. A priming step that specifically induces a T_{RM} cell precursor population that is poised to home to a specific

tissue could be particularly advantageous for a localized infection actively occurring within that tissue. In contrast, a more generalized mechanism of T_{RM} cell specification, in which less committed precursor cells enter tissues and differentiate into T_{RM} cells only in response to local tissue signals, might be more permissive for seeding of multiple, diverse tissues, as occurs in a systemic infection. Alternatively, it is possible that both models of T_{RM} cell fate specification could occur simultaneously during an infection, whereby each pathway induces functionally distinct subsets of T_{RM} cells.

In addition to finding substantial transcriptional differences between splenic and siIEL CD8$^+$ T cells at day 4 after infection, we also observed two transcriptionally distinct cell clusters within the siIEL CD8$^+$ T cell pool at day 4 after infection. Cells from one cluster expressed higher levels of genes associated with proliferation and effector differentiation and were less likely to develop into long-lived CD69$^+$CD103$^+$ T_{RM} cells when transferred into new recipients. By contrast, cells from the other cluster, marked by lower expression of IL-2Rα, exhibited a greater potential to give rise to T_{RM} cells upon adoptive transfer. Although it remains unknown whether this heterogeneity is a specific feature of the siIEL compartment or generalizable to T_{RM} cell differentiation in other nonlymphoid tissues, our analyses establish that analogous to the IL-2Rα^{lo} population present within the circulating CD8$^+$ T cell pool early in infection that contains the precursors of circulating memory cells (59, 60), bona fide T_{RM} cell precursors can be found within the IL-2Rα^{lo} cell subset present within the siIEL compartment at day 4 after infection. This finding represents an important step in understanding the ontogeny of T_{RM} cells after their arrival in the tissue that will likely inform future studies to identify early determinants of T_{RM} cell fate specification.

Whereas the heterogeneity within the circulating memory CD8$^+$ T cell pool is well characterized, heterogeneity among T_{RM} cells is much less clear. Some studies have reported tissue-specific differences in CD69 and CD103 expression by CD8$^+$ T cells, but it is unknown whether this heterogeneity represents functionally distinct subsets (18, 70–72). Our analyses identify two transcriptionally distinct cell clusters at days 60 and 90 after infection that exhibit unique functional capacities. One population, distinguished by higher expression of CD28 and IL-7Rα, expressed high levels of transcripts encoding inflammatory cytokines and exhibited an enhanced ability to produce cytokines in response to restimulation. In addition, this population exhibited higher expression of *Klf2*, which promotes tissue egress and recirculation. By contrast, the other population, characterized by lower CD28 and IL-7Rα expression, exhibited higher expression of transcripts encoding molecules that promote tissue retention, such as *Cxcr3* and *Klf3* (13, 73). Recent studies have revealed that the "tissue residency" of T_{RM} cells is not as permanent as previously thought; upon reactivation, T_{RM} cells harbor the potential to leave the tissues and join the circulating memory pool or form T_{RM} cell populations within secondary lymphoid organs (74, 75). Our findings suggest that this functionality may be restricted to a specific subset of T_{RM} cells that is better poised to leave the tissue. A recent study found that a subset of T_{RM} cells with high expression of the transcription factor Id3, which we also found to be more highly expressed within the CD28^{hi} T_{RM} population, exhibits an enhanced capacity to survive and give rise to circulating memory cells when adoptively transferred into new hosts (55). By contrast, the second T_{RM} cell subset might be more prone to remain within the tissue and mediate protective responses directly within

the tissue microenvironment. Moreover, in addition to revealing functionally distinct subsets within the T_{RM} cell pool, our transcriptional analyses have also elucidated a number of factors regulating the differentiation of these subsets. Analogous to our findings, a recent study provided evidence for distinct subsets of human T_{RM} cells, one with a greater potential for cytokine production and another with a higher proliferative potential in response to TCR stimulation (76).

Overall, our work has resulted in a single-cell transcriptomic dataset encompassing the gene expression patterns of circulating and siIEL CD8$^+$ T cells in response to viral infection. Our study reveals a core transcriptional program that is shared between circulating memory and T_{RM} cells in addition to key differences in the kinetics and magnitude of gene expression between these two memory cell subtypes, which should serve as a useful resource for elucidating new genes and pathways regulating T_{RM} cell differentiation. Our analyses demonstrate that CD8$^+$ T cells within the siIEL compartment become transcriptionally distinct from circulating cells rapidly upon entry into tissue and identify a subset of early siIEL CD8$^+$ T cells enriched for precursors of T_{RM} cells. Moreover, our study reveals previously unappreciated molecular and functional heterogeneity within the T_{RM} cell pool, underscoring the power and necessity of using a single-cell approach. This dataset should inform future studies aimed at improving our understanding of CD8$^+$ T cell differentiation and function, which may lead to strategies to optimize CD8$^+$ T cell responses to protect against microbial infection and cancer.

MATERIALS AND METHODS
Study design
The purpose of this study was to gain a broader understanding of the gene expression patterns that regulate CD8$^+$ T cell differentiation and heterogeneity in response to viral infection. To this end, we performed scRNA-seq on CD8$^+$ T cells in the spleen and small intestinal epithelium at various time points after viral infection to generate a dataset analyzing gene expression patterns over time in individual CD8$^+$ T cells. Analysis of this dataset revealed a subset of genes whose expression was enriched in CD8$^+$ T cells from the tissue, and the role of several of these factors in regulating the differentiation of T_{RM} CD8$^+$ T cells was validated by flow cytometric analysis of CD8$^+$ T cells with shRNA-mediated knockdown of these genes. In addition, validation of putative subsets of CD8$^+$ T cells within the tissue was performed by flow cytometric analysis, including sorting of individual putative subsets and assessment of function after ex vivo restimulation or adoptive transfer into secondary hosts. Information regarding the sample size and number of replicates for each experiment can be found in the relevant figure legend. All findings were successfully reproduced. No sample size calculations were performed; sample sizes were selected on the basis of previous studies performed in our lab. Mice were randomly allocated into groups before adoptive transfer of sorted IL-2Rα^{hi} or IL-2Rα^{lo} intraepithelial P14 T cells (Fig. 6). For scRNA-seq experiments, mice were randomly selected for P14 T cell harvesting at specific time points after infection. Randomization and blinding are not relevant to shRNA KD experiments or experiments involving cotransfer of $Ddx5^{-/-}$ and WT CD8$^+$ T cells, because P14 T cells transduced with retrovirus encoding shRNA against genes of interest and congenically distinct P14 T cells transduced with control retrovirus, or $Ddx5^{-/-}$ and WT

CD8$^+$ T cells, were cotransferred into the same animals (Figs. 2 and 5). For assessment of phenotype of adoptively transferred sorted IL-2Rα^{hi} or IL-2Rα^{lo} intraepithelial P14 T cells (Fig. 6), the investigator was aware of the cell type transferred into each recipient. No data were excluded from analysis, except for recipient mice that had rejected adoptively transferred P14 CD8$^+$ T cells.

Mice
All mice were housed under specific pathogen-free conditions in an American Association of Laboratory Animal Care–approved facility at the University of California, San Diego (UCSD), and all procedures were approved by the UCSD Institutional Animal Care and Use Committee. WT C57BL6/J (CD45.2$^+$) and P14 TCR transgenic (CD45.1 or CD45.1.2$^+$, both maintained on a C57BL6/J background) mice were bred at UCSD or purchased from the Jackson Laboratories. $Ddx5^{fl/fl}$ mice were obtained from Dr. Frances Fuller-Pace's laboratory (University of Dundee) and have been previously described (77). To obtain congenically distinct P14 $Ddx5^{fl/fl}$CD4-Cre$^+$ and P14 $Ddx5^{fl/fl}$CD4-Cre$^-$ mice, $Ddx5^{fl/fl}$ mice were crossed to P14 CD4-Cre$^+$ mice (either CD45.1$^+$ or CD45.2$^+$). All mice were used from 6 to 9 weeks of age, male mice were used as recipients, and male or female mice were used as donors in adoptive transfer experiments.

Antibodies, flow cytometry, and cell sorting
Cells were stained for 10 min on ice with the following antibodies: Vα2 (B20.1), CD8α (53-6.7), CD8β (YTS156.7.7), CD45.1 (A20), CD45.2 (104), CD44 (1 M7), CX3CR1 (SA011F11), CD127 (A7R34), CD27 (LG.3A10), CD69 (H1.2F3), CD103 (2E7), CD28 (37.51), CD25 (PC61), and KLRG1 (2F1/KLRG1) all purchased from BioLegend. In some experiments, cells were stained with H-2D^b GP$_{33–41}$ tetramer [obtained from the National Institutes of Health (NIH) Tetramer Core Facility] for 1 hour at room temperature before staining with cell surface antibodies. Samples were then stained in Fixable Viability Dye eFluor780 (Thermo Fisher Scientific) or Ghost Violet 510 (Tonbo Biosciences) at 1:1000 on ice for 10 min. For experiments with retroviral transduction of P14 T cells, cells were then fixed in 2% paraformaldehyde (Electron Microscopy Services) on ice for 45 min. For staining for Ezh2, cells were fixed and permeabilized using the FoxP3/Transcription Factor Staining Buffer Kit (Thermo Fisher Scientific) after staining with viability dye, before incubation with anti-Ezh2 antibody (11/Ezh2, BD Pharmingen) for 8 hours at 4°C. For assessment of cytokine production, cells were cultured in the presence of LCMV GP$_{33–41}$ peptide (GenScript) and Protein Transport Inhibitor Cocktail (Thermo Fisher Scientific) for 3 hours at 37°C. After cell surface and viability staining, cells were fixed and permeabilized using BD Cytofix/Cytoperm (BD Biosciences) for 30 min at room temperature before staining with anti–IFN-γ (XMG1.2), TNF-α (MP6-XT22), and IL-2 (JES6-5H4) antibodies (all from BioLegend) for 30 min on ice. For analysis, all samples were run on an Accuri C6, LSRFortessa, or LSRFortessa X-20 (BD Biosciences) or Novocyte (ACEA Biosciences). For sorting, all samples were run on an Influx, FACSAria Fusion, or FACSAria2 (BD Biosciences). BD FACS DIVA software (BD Biosciences) was used for data collection, and FlowJo software (BD Biosciences) was used for analysis of flow cytometry data.

Naïve T cell transfer and infection
Splenocytes were collected from naïve CD45.1$^+$ or CD45.1.2$^+$ P14 mice and stained with antibodies against Vα2, CD8, and CD45.1.

Vα2⁺CD8⁺CD45.1⁺ cells (1 × 10⁵) were adoptively transferred into congenically distinct WT recipients 1 day before infection with 2 × 10⁵ plaque-forming units (PFU) of LCMV Armstrong, injected intraperitoneally. For experiments where IEL were collected at 4 days after infection, 5 × 10⁵ Vα2⁺CD8⁺CD45.1⁺ P14 T cells were transferred. To distinguish circulating CD8⁺ T cells in nonlymphoid tissues from tissue-resident CD8⁺ T cells, 3 μg of CD8α was injected intravenously before euthanasia and dissection. Cells negative for injected CD8α (CD8α⁻ > 98%) were analyzed further.

CD8⁺ T cell isolation
For isolation of CD8⁺ T cells from the spleen, spleens were collected and dissociated to yield a cell suspension before treatment with Red Blood Cell Lysing Buffer Hybri-Max (Sigma-Aldrich). For isolation of CD8⁺ T cells from the small intestinal epithelium, Peyer's patches were removed, and the tissue was cut longitudinally and washed of luminal contents. The tissue was then cut into 1-cm pieces that were incubated while shaking in DTE buffer [dithioerythritol (1 μg/ml; Thermo Fisher Scientific) in 10% Hanks' balanced salt solution and 10% Hepes bicarbonate] at 37°C for 30 min. Cells within the supernatant were collected and passed through a 44/67% Percoll density gradient to enrich for lymphocytes.

10x Genomics library preparation and sequencing
Activated P14 T cells (CD8⁺Vα2⁺CD45.1⁺CD44⁺) were sorted from the spleen or siIEL compartment and resuspended in phosphate-buffered saline (PBS) + 0.04% (w/v) bovine serum albumin. About 10,000 cells per sample were loaded into Single Cell A chips (10x Genomics) and partitioned into Gel Bead In-Emulsions in a Chromium Controller (10x Genomics). Single-cell RNA libraries were prepared according to the 10x Genomics Chromium Single Cell 3′ Reagent Kits v2 User Guide and sequenced on a HiSeq 4000 (Illumina).

Generation of shRNA-encoding retrovirus, transduction of CD8⁺ T cells, and adoptive transfer for analysis of gene KD
shERWOOD-designed UltramiR sequences targeting *Junb*, *Nr4a2*, *Pnrc1*, *Fosl2*, or *Zfp36l2* (KD) or control (nontargeting) constructs in LMP-d Ametrine vector were purchased from transOMIC technologies. To generate retroviral particles, human embryonic kidney–293T cells were plated in 10-cm plates 1 day before transfection and individually transfected with 10 μg of each shRNA retroviral construct and 5 μg of pCL-Eco using TransIT-LT1 (Mirus). The retroviral supernatant was collected and pooled at 48 and 72 hours after transfection, in vitro–activated P14 T cells were transduced with retrovirus encoding KD shRNA, and congenically distinct in vitro–activated P14 T cells were transduced with control retrovirus. To activate P14 T cells in vitro, lymphocytes were collected from spleens and lymph nodes of naïve CD45.1⁺ and CD45.1.2⁺ P14 TCR transgenic mice and negatively enriched for CD8⁺ T cells using the CD8a⁺ T Cell Isolation Kit and LS MACS Columns (Miltenyi Biotec). CD8⁺ T cells (1 × 10⁶ per well) were plated in 48-well flat-bottom plates and precoated with goat anti-hamster IgG (100 μg/ml; H+L, Thermo Fisher Scientific), followed by 5 μg/ml each anti-CD3 (clone 3C11, BioXCell) and anti-CD28 (clone 37.51, BioXCell). Eighteen hours after activation, cells were transduced with retroviral supernatant supplemented with polybrene (8 μg/ml; Millipore) by spinfection for 90 min at 900 rcf (relative centrifugal force) at room temperature. After spinfection, the retroviral supernatant was removed and replaced with culture medium [Iscove's modified Dulbecco's medium

+ 10% fetal bovine serum (v/v) + 2 mM glutamine + penicillin (100 U/ml) + streptomycin (100 μg/ml) + 55 mM β-mercaptoethanol], and cells were rested for 2 hours at 37°C. Cells transduced with each individual construct were then pooled, washed three times with PBS, counted, and mixed to obtain a 1:1 ratio of transduced KD and transduced control cells, based on previously tested transduction efficiency of each retrovirus. Total P14 T cells (5 × 10⁵) were then adoptively transferred into congenically distinct hosts that were infected with 2 × 10⁵ PFU LCMV-Arm 1 hour later. Cells (1 × 10⁶) from this mixture were returned to culture with recombinant IL-2 (100 U/ml) and analyzed 18 hours later by flow cytometry to determine the input ratio of transduced KD/control P14 T cells. Twenty-two to 26 days after infection, splenocytes and siIEL were collected, as described above, and analyzed by flow cytometry to determine the ratio of KD/control cells within each subset of transduced P14 T cells.

Statistical analysis of flow cytometry data
Statistical analysis of flow cytometry data was performed using Prism software (GraphPad). $P < 0.05$ was considered significant. Statistical details for each experiment are provided within the relevant figure legends and the raw data file.

Quantitative and statistical analysis of scRNA-seq data
scRNA-seq mapping
Reads from scRNA-seq were aligned to mm10 and collapsed into unique molecular identifier (UMI) counts using the 10x Genomics Cell Ranger software (version 2.1.0). All samples had sufficient numbers of genes detected (>1000), a high percentage of reads mapped to the genome (>70%), and a sufficient number of cells detected (>1000).
Cell and gene filtering
Raw cell-reads were loaded to R using the cellrangerRkit package. The scRNA-seq dataset was then further filtered on the basis of gene numbers and mitochondria gene counts to total counts ratio. To ensure that the samples with more cells would not dominate the downstream analysis, we randomly selected a portion of the cells that passed filtering for downstream analysis. We randomly selected ~2000 cells from each library for downstream analysis. After cell filtering and sampling, we filtered genes by removing genes that did not express >1 UMI in more than 1% of the total cells.
scRNA-seq dataset normalization and preprocessing
Five cell-gene matrices were generated as follows:

   1) Raw UMI matrix.

   2) UPM matrix. The raw UMI matrix was normalized to get UMIs per million reads (UPM) and was then log₂-transformed. All downstream differential analysis was based on the UPM matrix. The prediction models were also based on the UPM matrix, as other normalizations are very time consuming for large datasets.

   3) MAGIC (Markov Affinity-based Graph Imputation of Cells) matrix. The UPM matrix was further permuted by MAGIC (*78*). R package Rmagic 1.0.0 was used, and all options were kept as default. MAGIC aims to correct the dropout effect of scRNA-seq data; thus, we used the MAGIC-corrected matrix for visualizing the gene expression pattern rather than using the UPM matrix. All gene expression heatmaps and gene expression overlaid on tSNE plots were based on the MAGIC matrix.

   4) Supercell matrix. We merged 50 cells to create a "super" cell and used the supercell matrix as the input for WGCNA (weighted gene correlation network analysis) and cell-type annotation analysis.

This approach enabled us to bypass the issue of gene dropouts with scRNA-seq and is equivalent to performing WGCNA on thousands of pseudobulk samples. We first calculated the mutual nearest neighbor network with k set to 15, and then cells that were not mutual nearest neighbors with any other cells were removed as outliers. We randomly selected "n" cells in the UPM matrix as the seed for supercells. The expression of each supercell was equal to the average expression of its seed and the 50 nearest neighbor cells of its seed. We derived 7400 supercells from the dataset, so each single cell was covered ~10 times.

scRNA-seq dataset dimension reduction

Top variable genes, principal components analysis (PCA), and tSNE were calculated by Seurat version 2.3.4 functions: FindVariableGenes, RunPCA, and RunTSNE (*79*). Only the top 3000 genes were considered in the PCA calculation and only the top 25 PCs were used in tSNE. Louvain clustering was performed by Seurat's FindClusters function based on the top 25 PCs, with resolution set to 2. UMAP was calculated by R packages umap_0.2 with default setting.

Differential gene expression analysis

DE genes were identified by performing pairwise comparison using two-sided Wilcox test and the FindAllMarkers function of Seurat. The threshold for DE genes was $P < 0.05$ and an absolute fold change of >2.

WGCNA analysis

We performed WGCNA (version 1.63) analysis on spleen cells alone, siIEL cells alone, or all cells considered together. The supercell matrices were used as the input to boost performance. Only the top 5000 variable genes were considered in this analysis. SoftPower was set to 9, and the signed adjacency matrix was calculated for gene module identification. Genetree clustering and eigengene clustering were based on average hierarchical clustering. Module cut height was set to 0.1. GO analysis of the gene module was performed by compareClusterfunction from R package clusterProfiler 3.2.14. Reference database was org,Hs.eg.db 3.4.0 from Bioconductor and options were fun = "enrichGO", pAdjustMethod = "fdr", pvalueCutoff = 0.01, and qvalueCutoff = 0.05 .

Annotating single cells with bulk RNA-seq signatures

The $\log_2$ transcripts per million data from bulk RNA-seq datasets were compared with the scRNA-seq supercell matrix. Bulk cell population RNA-seq samples were first grouped into different sets according to their mutual similarities. For each bulk RNA-seq sample set, the mean expression was first calculated. The first correlation was calculated between all the supercells and the mean expression from the bulk RNA-seq dataset. On the basis of the distribution of the first correlation, we were able to identify a group of supercells that were most similar to the mean expression of the bulk sample. To further identify the small differences between bulk RNA-seq expression within a given set, we removed the set mean from the bulk RNA-seq and the mean from the most similar group of supercells and then calculated the second correlation between the supercells and bulk RNA-seq. On the basis of the second correlation, we annotated the supercells with each bulk sample label.

PAGA trajectory analysis

The single-cell trajectories were constructed using the PAGA algorithm (*54*) implemented in the scanpy package (*80*). The UMI counts of the filtered cells and genes (filtered by the same approach mentioned above) were normalized by sequence depth before trajectory construction. In the construction, the knn-graphs were built with the *scanpy.pp.neighbors* function (n_neighbors = 7 and n_pcs = 20), and PAGA graphs were constructed using the *scanpy.tl.paga* function with default settings. In the PAGA graphs, each node represents a cell partition (a group of cells), and the edges between nodes represent the connection between these nodes measured by PAGA, whereas the strength of the edge describes the degree of connection (connectivity), which varies from 0 to 1. Only the edges with connectivity larger than 0.2 were shown in the final PAGA graphs, and graphs were based on clusters defined with Louvain clustering.

SUPPLEMENTARY MATERIALS

immunology.sciencemag.org/cgi/content/full/5/47/eaaz6894/DC1

Fig. S1. Sorting of P14 CD8^{+} T cells from spleen and siIEL for scRNA-seq.

Fig. S2. Circulating and siIEL CD8^{+} T cells are transcriptionally distinct at all time points after infection.

Fig. S3. Differential gene expression of circulating and siIEL CD8^{+} T cells at day 4 after infection.

Fig. S4. Shared core transcriptional program among splenic and siIEL CD8^{+} T cells.

Fig. S5. Components of the T$_{RM}$ cell–enriched transcriptional signature.

Fig. S6. shRNA knockdown of putative regulators of T$_{RM}$ cell differentiation.

Fig. S7. PAGA trajectory analysis of T$_{RM}$ cell differentiation.

Table S1. DE genes by splenic and siIEL CD8^{+} T cells at day 4 after infection.

Table S2. Genes in Spleen and IEL Modules.

Table S3. Genes in Combined Modules.

Table S4. DE genes by day 60 versus day 90 T$_{CM}$-like cells.

Table S5. DE genes by Cluster 3 versus Cluster 29 cells.

Table S6. DE genes by Cluster 17 versus Cluster 19 cells.

Table S7. DE genes by Cluster 16 versus Cluster 20 cells.

Table S8. Raw data file (Excel spreadsheet).

View/request a protocol for this paper from *Bio-protocol*.

REFERENCES AND NOTES

1. J. T. Chang, E. J. Wherry, A. W. Goldrath, Molecular regulation of effector and memory T cell differentiation. *Nat. Immunol.* **15**, 1104–1115 (2014).

2. F. Sallusto, D. Lenig, R. Förster, M. Lipp, A. Lanzavecchia, Two subsets of memory T lymphocytes with distinct homing potentials and effector functions. *Nature* **401**, 708–712 (1999).

3. S. C. Jameson, D. Masopust, Understanding subset diversity in T cell memory. *Immunity* **48**, 214–226 (2018).

4. K. D. Omilusik, M. S. Nadjsombati, L. A. Shaw, B. Yu, J. J. Milner, A. W. Goldrath, Sustained Id2 regulation of E proteins is required for terminal differentiation of effector CD8^{+} T cells. *J. Exp. Med.* **215**, 773–783 (2018).

5. J. A. Olson, C. McDonald-Hyman, S. C. Jameson, S. E. Hamilton, Effector-like CD8^{+} T cells in the memory population mediate potent protective immunity. *Immunity* **38**, 1250–1260 (2013).

6. H. Hikono, J. E. Kohlmeier, S. Takamura, S. T. Wittmer, A. D. Roberts, D. L. Woodland, Activation phenotype, rather than central– or effector–memory phenotype, predicts the recall efficacy of memory CD8^{+} T cells. *J. Exp. Med.* **204**, 1625–1636 (2007).

7. S. N. Mueller, L. K. Mackay, Tissue-resident memory T cells: Local specialists in immune defence. *Nat. Rev. Immunol.* **16**, 79–89 (2016).

8. S. Ariotti, M. A. Hogenbirk, F. E. Dijkgraaf, L. L. Visser, M. E. Hoekstra, J. Y. Song, H. Jacobs, J. B. Haanen, Skin-resident memory CD8^{+} T cells trigger a state of tissue-wide pathogen alert. *Science* **346**, 101–105 (2014).

9. X. Jiang, R. A. Clark, L. Liu, A. J. Wagers, R. C. Fuhlbrigge, T. S. Kupper, Skin infection generates non-migratory memory CD8^{+} T$_{RM}$ cells providing global skin immunity. *Nature* **483**, 227–231 (2013).

10. J. M. Schenkel, K. A. Fraser, L. K. Beura, K. E. Pauken, V. Vezys, D. Masopust, Resident memory CD8 T cells trigger protective innate and adaptive immune responses. *Science* **346**, 98–101 (2014).

11. S. L. Park, A. Buzzai, J. Rautela, J. L. Hor, K. Hochheiser, M. Effern, N. McBain, T. Wagner, J. Edwards, R. McConville, J. S. Wilmott, R. A. Scolyer, T. Tüting, U. Palendira, D. Gyorki, S. N. Mueller, N. D. Huntington, S. Bedoui, M. Hölzel, L. K. Mackay, J. Waithman, T. Gebhardt, Tissue-resident memory CD8^{+} T cells promote melanoma–immune equilibrium in skin. *Nature* **565**, 366–371 (2019).

12. L. K. Mackay, M. Minnich, N. Kragten, Y. Liao, B. Nota, C. Seillet, A. Zaid, K. Man, S. Preston, L. S. Bell, S. Andrews, M. D. Diaz-Munoz, S. J. Cook, A. Corcoran, M. Turner, D. Freestone, A. Braun, E. Wynne-Jones, F. M. Behr, R. Stark, D. G. Pellici, D. I. Godfrey, G. T. Belz, M. Pellegrini, T. Gebhardt, M. Busslinger, W. Shi, F. R. Carbone, R. van Lier, A. Kallies, K. van Gisbergen, Hobit and Blimp1 instruct a universal transcriptional program of tissue residency in lymphocytes. *Science* **352**, 459–463 (2016).

13. L. K. Mackay, A. Rahimpour, J. Z. Ma, N. Collins, A. T. Stock, M.-L. Hafon, J. Vega-Ramos, P. Lauzurica, S. N. Mueller, M. Stefanovic, D. C. Tscharke, W. R. Heath, M. Inouye, F. R. Carbone, T. Gebhardt, The developmental pathway for CD103+CD8+ tissue-resident memory T cells of skin. *Nat. Immunol.* **14**, 1294–1301 (2013).

14. C. N. Skon, J.-Y. Lee, K. G. Anderson, D. Masopust, K. A. Hogquist, S. C. Jameson, Transcriptional downregulation of S1pr1 is required for the establishment of resident memory CD8+ T cells. *Nat. Immunol.* **14**, 1285–1293 (2013).

15. L. K. Mackay, E. Wynne-Jones, D. Freestone, D. G. Pellicci, L. A. Mielke, D. M. Newman, A. Braun, F. Masson, A. Kallies, G. T. Belz, F. R. Carbone, T-box transcription factors combine with the cytokines TGF-β and IL-15 to control tissue-resident memory T cell fate. *Immunity* **43**, 1101–1111 (2015).

16. J. J. Milner, C. Toma, B. Yu, K. Zhang, K. Omilusik, A. T. Phan, D. Wang, A. J. Getzler, T. Nguyen, S. Crotty, W. Wang, M. E. Pipkin, A. W. Goldrath, Runx3 programs CD8+ T cell residency in non-lymphoid tissues and tumours. *Nature* **552**, 253–257 (2017).

17. J. J. Milner, A. W. Goldrath, Transcriptional programming of tissue-resident memory CD8+ T cells. *Curr. Opin. Immunol.* **51**, 162–169 (2018).

18. L. M. Wakim, A. Woodward-Davis, R. Liu, Y. Hu, J. Villadangos, G. Smyth, M. J. Bevan, The molecular signature of tissue resident memory CD8 T cells isolated from the brain. *J. Immunol.* **189**, 3462–3471 (2012).

19. D. Fernandez-Ruiz, W. Y. Ng, L. E. Holz, J. Z. Ma, A. Zaid, Y. C. Wong, L. S. Lau, V. Mollard, A. Cozijnsen, N. Collins, J. Li, G. M. Davey, Y. Kato, S. Devi, R. Skandari, M. Pauley, J. H. Manton, D. I. Godfrey, A. Braun, S. S. Tay, P. S. Tan, D. G. Bowen, F. Koch-Nolte, B. Rissiek, F. R. Carbone, B. S. Crabb, M. Lahoud, I. A. Cockburn, S. N. Mueller, P. Bertolino, G. I. McFadden, I. Caminschi, W. R. Heath, Liver-Resident Memory CD8+ T cells form a front-line defense against malaria liver-stage infection. *Immunity* **45**, 889–902 (2016).

20. B. Kakaradov, J. Arsenio, C. E. Widjaja, Z. He, S. Aigner, P. J. Metz, B. Yu, E. J. Wehrens, J. Lopez, S. H. Kim, E. I. Zuniga, A. W. Goldrath, J. T. Chang, G. W. Yeo, Early transcriptional and epigenetic regulation of CD8+ T cell differentiation revealed by single-cell RNA sequencing. *Nat. Immunol.* **18**, 422–432 (2017).

21. E. Azizi, A. J. Carr, G. Plitas, A. E. Cornish, C. Konopacki, S. Prabhakaran, J. Nainys, K. Wu, V. Kiseliovas, M. Setty, K. Choi, R. M. Fromme, P. Dao, P. T. McKenney, R. C. Wasti, K. Kadaveru, L. Mazutis, A. Y. Rudensky, D. Pe'er, Single-cell map of diverse immune phenotypes in the breast tumor microenvironment. *Cell* **174**, 1293–1308.e36 (2018).

22. P. Savas, B. Virassamy, C. Ye, A. Salim, C. P. Mintoff, F. Caramia, R. Salgado, D. J. Byrne, Z. L. Teo, S. Dushyanthen, A. Byrne, L. Wein, S. J. Luen, C. Poliness, S. S. Nightingale, A. S. Skandarajah, D. E. Gyorki, C. M. Thornton, P. A. Beavis, S. B. Fox; Kathleen Cuningham Foundation Consortium for Research into Familial Breast Cancer (kConFab), P. K. Darcy, T. P. Speed, L. K. Mackay, P. J. Neeson, S. Loi, Single-cell profiling of breast cancer T cells reveals a tissue-resident memory subset associated with improved prognosis. *Nat. Med.* **24**, 986–993 (2018).

23. J. Brummelman, E. M. C. Mazza, G. Alvisi, F. S. Colombo, A. Grilli, J. Mikulak, D. Mavilio, M. Alloisio, F. Ferrari, E. Lopci, P. Novellis, G. Veronesi, E. Lugli, High-dimensional single cell analysis identifies stem-like cytotoxic CD8+ T cells infiltrating human tumors. *J. Exp. Med.* **215**, 2520–2535 (2018).

24. J. T. Gaublomme, N. Yosef, Y. Lee, R. S. Gertner, L. V. Yang, C. Wu, P. P. Pandolfi, T. Mak, R. Satija, A. K. Shalek, V. K. Kuchroo, H. Park, A. Regev, Single-cell genomics unveils critical regulators of Th17 cell pathogenicity. *Cell* **163**, 1400–1412 (2015).

25. C. Zheng, L. Zheng, J.-K. Yoo, H. Guo, Y. Zhang, X. Guo, B. Kang, R. Hu, J. Y. Huang, Q. Zhang, Z. Liu, M. Dong, X. Hu, W. Ouyang, J. Peng, Z. Zhang, Landscape of infiltrating T cells in liver cancer revealed by single-cell sequencing. *Cell* **169**, 1342–1356.e16 (2017).

26. D. Karamitros, B. Stoilova, Z. Aboukhalil, F. Hamey, A. Reinisch, M. Samitsch, L. Quek, G. Otto, E. Repapi, J. Doondeea, B. Usukhbayar, J. Calvo, S. Taylor, N. Goardon, E. Six, F. Pflumio, C. Porcher, R. Majeti, B. Göttgens, P. Vyas, Single-cell analysis reveals the continuum of human lympho-myeloid progenitor cells. *Nat. Immunol.* **19**, 85–97 (2018).

27. A. Schlitzer, V. Sivakamasundari, J. Chen, H. R. B. Sumatoh, J. Schreuder, J. Lum, B. Malleret, S. Zhang, A. Larbi, F. Zolezzi, L. Renia, M. Poidinger, S. Naik, E. W. Newell, P. Robson, F. Ginhoux, Identification of cDC1- and cDC2-committed DC progenitors reveals early lineage priming at the common DC progenitor stage in the bone marrow. *Nat. Immunol.* **16**, 718–728 (2015).

28. E. Mass, I. Ballesteros, M. Farlik, F. Halbritter, P. Günther, L. Crozet, C. E. Jacome-Galarza, K. Händler, J. Klughammer, Y. Kobayashi, E. Gomez-Perdiguero, J. L. Schultze, M. Beyer, C. Bock, F. Geissmann, Specification of tissue-resident macrophages during organogenesis. *Science* **353**, aaf4238 (2016).

29. A.-C. Villani, R. Satija, G. Reynolds, S. Sarkizova, K. Shekhar, J. Fletcher, M. Griesbeck, A. Butler, S. Zheng, S. Lazo, L. Jardine, D. Dixon, E. Stephenson, E. Nilsson, I. Grundberg, D. McDonald, A. Filby, W. Li, P. L. De Jager, O. Rozenblatt-Rosen, A. A. Lane, M. Haniffa, A. Regev, N. Hacohen, Single-cell RNA-seq reveals new types of human blood dendritic cells, monocytes, and progenitors. *Science* **356**, eaah4573 (2017).

30. D. Masopust, V. Vezys, E. J. Wherry, D. L. Barber, R. Ahmed, Cutting edge: Gut microenvironment promotes differentiation of a unique memory CD8 T cell population. *J. Immunol.* **176**, 2079–2083 (2006).

31. H. B. da Silva, L. K. Beura, H. Wang, E. A. Hanse, R. Gore, M. C. Scott, D. A. Walsh, K. E. Block, R. Fonseca, Y. Yan, K. L. Hippen, B. R. Blazar, D. Masopust, A. Kelekar, L. Vulchanova, K. A. Hogquist, S. C. Jameson, The purinergic receptor P2RX7 directs metabolic fitness of long-lived memory CD8+ T cells. *Nature* **559**, 264–268 (2018).

32. Y. Pan, T. Tian, C. O. Park, S. Y. Lofftus, S. Mei, X. Liu, C. Luo, J. T. O'Malley, A. Gehad, J. E. Teague, S. J. Divito, R. Fuhlbrigge, P. Puigserver, J. G. Krueger, G. S. Hotamisligil, R. A. Clark, T. S. Kupper, Survival of tissue-resident memory T cells requires exogenous lipid uptake and metabolism. *Nature* **543**, 252–256 (2017).

33. K. D. Omilusik, J. A. Best, B. Yu, S. Goossens, A. Weidemann, J. V. Nguyen, E. Seuntjens, A. Stryjewska, C. Zweier, R. Roychoudhuri, L. Gattinoni, L. M. Bird, Y. Higashi, H. Kondoh, D. Huylebroeck, J. Haigh, A. W. Goldrath, Transcriptional repressor ZEB2 promotes terminal differentiation of CD8+ effector and memory T cell populations during infection. *J. Exp. Med.* **212**, 2027–2039 (2015).

34. R. Roychoudhuri, D. Clever, P. Li, Y. Wakabayashi, K. M. Quinn, C. A. Klebanoff, Y. Ji, M. Sukumar, R. L. Eil, Z. Yu, R. Spolski, D. C. Palmer, J. H. Pan, S. J. Patel, D. C. Macallan, G. Fabozzi, H.-Y. Shih, Y. Kanno, A. Muto, J. Zhu, L. Gattinoni, J. J. O'Shea, K. Okkenhaug, K. Igarashi, W. J. Leonard, N. P. Restifo, BACH2 regulates CD8+ T cell differentiation by controlling access of AP-1 factors to enhancers. *Nat. Immunol.* **17**, 851–860 (2016).

35. C. E. Widjaja, J. G. Olvera, P. J. Metz, A. T. Phan, J. N. Savas, G. de Bruin, Y. Leestemaker, C. R. Berkers, A. de Jong, B. I. Florea, K. Fisch, J. Lopez, S. H. Kim, D. A. Garcia, S. Searles, J. D. Bui, A. N. Chang, J. R. Yates III, A. W. Goldrath, H. S. Overkleeft, H. Ovaa, J. T. Chang, Proteasome activity regulates CD8+ T lymphocyte metabolism and fate specification. *J. Clin. Invest.* **127**, 3609–3623 (2017).

36. D. J. Puleston, H. Zhang, T. J. Powell, E. Lipina, S. Sims, I. Panse, A. S. Watson, V. Cerundolo, A. R. Townsend, P. Klenerman, A. K. Simon, Autophagy is a critical regulator of memory CD8+ T cell formation. *eLife* **3**, e03706 (2014).

37. C. S. Boddupalli, S. Nair, S. M. Gray, H. N. Nowyhed, R. Verma, J. A. Gibson, C. Abraham, D. Narayan, J. Vasquez, C. C. Hedrick, R. A. Flavell, K. M. Dhodapkar, S. M. Kaech, M. V. Dhodapkar, ABC transporters and NR4A1 identify a quiescent subset of tissue-resident memory T cells. *J. Clin. Invest.* **126**, 3905–3916 (2016).

38. A. Zaid, L. K. Mackay, A. Rahimpour, A. Braun, M. Veldhoen, F. R. Carbone, J. H. Manton, W. R. Heath, S. N. Mueller, Persistence of skin-resident memory T cells within an epidermal niche. *Proc. Natl. Acad. Sci.* **111**, 5307–5312 (2014).

39. C. Li, B. Zhu, Y. M. Son, Z. Wang, L. Jiang, M. Xiang, Z. Ye, K. E. Beckermann, Y. Wu, J. W. Jenkins, P. J. Siska, B. G. Vincent, Y. S. Prakash, T. Peikert, B. T. Edelson, R. Taneja, M. H. Kaplan, J. C. Rathmell, H. Dong, T. Hitosugi, J. Sun, The transcription factor Bhlhe40 programs mitochondrial regulation of resident CD8+ T cell fitness and functionality. *Immunity* **51**, 491–507.e7 (2019).

40. T. Sekiya, I. Kashiwagi, R. Yoshida, T. Fukaya, R. Morita, A. Kimura, H. Ichinose, D. Metzger, P. Chambon, A. Yoshimura, Nr4a receptors are essential for thymic regulatory T cell development and immune homeostasis. *Nat. Immunol.* **14**, 230–237 (2013).

41. T. Sekiya, I. Kashiwagi, N. Inoue, R. Morita, S. Hori, H. Waldmann, A. Y. Rudensky, H. Ichinose, D. Metzger, P. Chambon, A. Yoshimura, The nuclear orphan receptor Nr4a2 induces Foxp3 and regulates differentiation of CD4+ T cells. *Nat. Commun.* **2**, 269 (2011).

42. B. J. E. Raveney, S. Oki, T. Yamamura, Nuclear receptor NR4A2 orchestrates Th17 cell-mediated autoimmune inflammation via IL-21 signalling. *PLOS ONE* **8**, e56595 (2013).

43. Y. Doi, S. Oki, T. Ozawa, H. Hohjoh, S. Miyake, T. Yamamura, Orphan nuclear receptor NR4A2 expressed in T cells from multiple sclerosis mediates production of inflammatory cytokines. *Proc. Natl. Acad. Sci. U.S.A.* **105**, 8381–8386 (2008).

44. J. P. Scott-Browne, I. F. López-Moyado, S. Trifari, V. Wong, L. Chavez, A. Rao, R. M. Pereira, Dynamic changes in chromatin accessibility occur in CD8+ T cells responding to viral infection. *Immunity* **45**, 1327–1340 (2016).

45. T. M. Carr, J. D. Wheaton, G. M. Houtz, M. Ciofani, JunB promotes Th17 cell identity and restrains alternative CD4+ T-cell programs during inflammation. *Nat. Commun.* **8**, 301 (2017).

46. Z. Hasan, S.-i. Koizumi, D. Sasaki, H. Yamada, N. Arakaki, Y. Fujihara, S. Okitsu, H. Shirahata, H. Ishikawa, JunB is essential for IL-23-dependent pathogenicity of Th17 cells. *Nat. Commun.* **8**, 15628 (2017).

47. M. Ciofani, A. Madar, C. Galan, M. Sellars, K. Mace, F. Pauli, A. Agarwal, W. Huang, C. N. Parkurst, M. Muratet, K. M. Newberry, S. Meadows, A. Greenfield, Y. Yang, P. Jain, F. K. Kirigin, C. Birchmeier, E. F. Wagner, K. M. Murphy, R. M. Myers, R. Bonneau, D. R. Littman, A validated regulatory network for Th17 cell specification. *Cell* **151**, 289–303 (2012).

48. S. M. Kaech, J. T. Tan, E. J. Wherry, B. T. Konieczny, C. D. Surh, R. Ahmed, Selective expression of the interleukin 7 receptor identifies effector CD8 T cells that give rise to long-lived memory cells. *Nat. Immunol.* **4**, 1191–1198 (2003).

49. N. S. Joshi, W. Cui, A. Chandele, H. K. Lee, D. R. Urso, J. Hagman, L. Gapin, S. M. Kaech, Inflammation directs memory precursor and short-lived effector CD8+ T cell fates via the graded expression of T-bet transcription factor. *Immunity* **27**, 281–295 (2007).

50. S. Sarkar, V. Kalia, W. N. Haining, B. T. Konieczny, S. Subramaniam, R. Ahmed, Functional and genomic profiling of effector CD8 T cell subsets with distinct memory fates. *J. Exp. Med.* **205**, 625–640 (2008).

51. C. Gerlach, E. A. Moseman, S. M. Loughhead, D. Alvarez, A. J. Zwijnenburg, L. Waanders, R. Garg, J. C. de la Torre, U. H. von Andrian, The chemokine receptor CX3CR1 defines three antigen-experienced CD8 T cell subsets with distinct roles in immune surveillance and homeostasis. *Immunity* **45**, 1270–1284 (2016).

52. E. J. Wherry, V. Teichgräber, T. C. Becker, D. Masopust, S. M. Kaech, R. Antia, U. H. von Andrian, R. Ahmed, Lineage relationship and protective immunity of memory CD8 T cell subsets. *Nat. Immunol.* **4**, 225–234 (2003).

53. M. E. Murphy, The HSP70 family and cancer. *Carcinogenesis* **34**, 1181–1188 (2013).

54. F. A. Wolf, F. K. Hamey, M. Plass, J. Solana, J. S. Dahlin, B. Göttgens, N. Rajewsky, L. Simon, F. J. Theis, PAGA: Graph abstraction reconciles clustering with trajectory inference through a topology preserving map of single cells. *Genome Biol.* **20**, 59 (2019).

55. J. J. Milner, C. Toma, Z. He, N. S. Kurd, Q. P. Nguyen, B. McDonald, L. Quezada, C. E. Widjaja, D. A. Witherden, J. T. Crowl, G. W. Yeo, J. T. Chang, K. D. Omilusik, A. W. Goldrath, Functional delineation of tissue-resident CD8+ T cell heterogeneity during infection and cancer. bioRxiv 2020.03.05.979146 [**Preprint**]. 6 March 2020. https://doi.org/10.1101/2020.03.05.979146.

56. C. Y. Yang, J. A. Best, J. Knell, E. Yang, A. D. Sheridan, A. K. Jesionek, H. S. Li, R. R. Rivera, K. C. Lind, L. M. D'Cruz, S. S. Watowich, C. Murre, A. W. Goldrath, The transcriptional regulators Id2 and Id3 control the formation of distinct memory CD8+ T cell subsets. *Nat. Immunol.* **12**, 1221–1229 (2011).

57. Y. Ji, Z. Pos, M. Rao, C. A. Klebanoff, Z. Yu, M. Sukumar, R. N. Reger, D. C. Palmer, Z. A. Borman, P. Muranski, E. Wang, D. S. Schrump, F. M. Marincola, N. P. Restifo, L. Gattinoni, Repression of the DNA-binding inhibitor Id3 by Blimp-1 limits the formation of memory CD8+ T cells. *Nat. Immunol.* **12**, 1230–1237 (2011).

58. F. Salerno, S. Engels, M. Biggelaar, F. P. J. Alphen, A. Guislain, W. Zhao, D. L. Hodge, S. E. Bell, J. P. Medema, M. Lindern, M. Turner, H. A. Young, M. C. Wolkers, Translational repression of pre-formed cytokine-encoding mRNA prevents chronic activation of memory T cells. *Nat. Immunol.* **19**, 828–837 (2018).

59. J. Arsenio, B. Kakaradov, P. J. Metz, S. H. Kim, G. W. Yeo, J. T. Chang, Early specification of CD8+ T lymphocyte fates during adaptive immunity revealed by single-cell gene-expression analyses. *Nat. Immunol.* **15**, 365–372 (2014).

60. V. Kalia, S. Sarkar, S. Subramaniam, W. N. Haining, K. A. Smith, R. Ahmed, Prolonged interleukin-2Rα expression on virus-specific CD8+ T cells favors terminal-effector differentiation in vivo. *Immunity* **32**, 91–103 (2010).

61. N. A. Vasilevsky, C. E. Ruby, P. J. Hurlin, A. D. Weinberg, OX40 engagement stabilizes Mxd4 and Mnt protein levels in antigen-stimulated T cells leading to an increase in cell survival. *Eur. J. Immunol.* **41**, 1024–1034 (2011).

62. C. Chappell, C. Beard, J. Altman, R. Jaenisch, J. Jacob, DNA methylation by DNA methyltransferase 1 is critical for effector CD8 T cell expansion. *J. Immunol.* **176**, 4562–4572 (2006).

63. S. M. Gray, R. A. Amezquita, T. Guan, S. H. Kleinstein, S. M. Kaech, Polycomb repressive complex 2-mediated chromatin repression guides effector CD8+ T cell terminal differentiation and loss of multipotency. *Immunity* **46**, 596–608 (2017).

64. S. L. Park, A. Zaid, J. L. Hor, S. N. Christo, J. E. Prier, B. Davies, Y. O. Alexandre, J. L. Gregory, T. A. Russell, T. Gebhardt, F. R. Carbone, D. C. Tscharke, W. R. Heath, S. N. Mueller, L. K. Mackay, Local proliferation maintains a stable pool of tissue-resident memory T cells after antiviral recall responses. *Nat. Immunol.* **19**, 183–191 (2018).

65. L. K. Beura, J. S. Mitchell, E. A. Thompson, J. M. Schenkel, J. Mohammed, S. Wijeyesinghe, R. Fonseca, B. J. Burbach, H. D. Hickman, V. Vezys, B. T. Fife, D. Masopust, Intravital mucosal imaging of CD8+ resident memory T cells shows tissue-autonomous recall responses that amplify secondary memory. *Nat. Immunol.* **19**, 173–182 (2018).

66. S. Cheuk, H. Schlums, I. G. Sérézal, E. Martini, S. C. Chiang, N. Marquardt, A. Gibbs, E. Detlofsson, A. Introini, M. Forkel, C. Höög, A. Tjernlund, J. Michaëlsson, L. Folkersen, J. Mjösberg, L. Blomqvist, M. Ehrström, M. Ståhle, Y. T. Bryceson, L. Eidsmo, CD49a expression defines tissue-resident CD8+ T cells poised for cytotoxic function in human skin. *Immunity* **46**, 287–300 (2017).

67. J. T. Chang, V. Palaivel, I. Kinjyo, F. Schambach, A. M. Intlekofer, A. Banerjee, S. A. Longworth, K. E. Vinup, P. Mrass, J. Oliaro, N. Killeen, J. S. Orange, S. M. Russell, W. Weninger, S. L. Reiner, Asymmetric T lymphocyte division in the initiation of adaptive immune responses. *Science* **315**, 1687–1691 (2007).

68. O. Gaide, R. O. Emerson, X. Jiang, N. Gulati, S. Nizza, C. Desmarais, H. Robins, J. G. Krueger, R. A. Clark, T. S. Kupper, Common clonal origin of central and resident memory T cells following skin immunization. *Nat. Med.* **21**, 647–653 (2015).

69. S. Iborra, M. Martínez-López, S. C. Khouili, M. Enamorado, F. J. Cueto, R. Conde-Garrosa, C. del Fresno, D. Sancho, Optimal generation of tissue-resident but not circulating memory T cells during viral infection requires crosspriming by DNGR-1+ dendritic cells. *Immunity* **45**, 847–860 (2016).

70. E. M. Steinert, J. M. Schenkel, K. A. Fraser, L. K. Beura, L. S. Manlove, B. Z. Igyártó, P. J. Southern, D. Masopust, Quantifying memory CD8 T cells reveals regionalization of immunosurveillance. *Cell* **161**, 737–749 (2015).

71. T. Bergsbaken, M. J. Bevan, P. J. Fink, Local inflammatory cues regulate differentiation and persistence of CD8+ tissue-resident memory T cells. *Cell Rep.* **19**, 114–124 (2017).

72. T. Bergsbaken, M. J. Bevan, Proinflammatory microenvironments within the intestine regulate the differentiation of tissue-resident CD8+ T cells responding to infection. *Nat. Immunol.* **16**, 406–414 (2015).

73. G. T. Hart, K. A. Hogquist, S. C. Jameson, Krüppel-like factors in lymphocyte biology. *J. Immunol.* **188**, 521–526 (2012).

74. R. Fonseca, L. K. Beura, C. F. Quarnstrom, H. E. Ghoneim, Y. Fan, C. C. Zebley, M. C. Scott, N. J. Fares-Frederickson, S. Wijeyesinghe, E. A. Thompson, H. B. da Silva, V. Vezys, B. Youngblood, D. Masopust, Developmental plasticity allows outside-in immune responses by resident memory T cells. *Nat. Immunol.* **21**, 412–421 (2020).

75. L. K. Beura, S. Wijeyesinghe, E. A. Thompson, M. G. Macchietto, P. C. Rosato, M. J. Pierson, J. M. Schenkel, J. S. Mitchell, V. Vezys, B. T. Fife, S. Shen, D. Masopust, T cells in nonlymphoid tissues give rise to lymph-node-resident memory T cells. *Immunity* **48**, 327–338.e5 (2018).

76. B. V. Kumar, R. Kratchmarov, M. Miron, D. J. Carpenter, T. Senda, H. Lerner, A. Friedman, S. L. Reiner, D. L. Farber, Functional heterogeneity of human tissue-resident memory T cells based on dye efflux capacities. *JCI Insight* **3**, 123568 (2018).

77. G. J. Bates, S. M. Nicol, B. J. Wilson, A. F. Jacobs, J. C. Bourdon, J. Wardrop, D. J. Gregory, D. P. Lane, N. D. Perkins, F. V. Fuller-Pace, The DEAD box protein p68: A novel transcriptional coactivator of the p53 tumour suppressor. *EMBO J.* **24**, 543–553 (2005).

78. D. van Dijk, R. Sharma, J. Nainys, K. Yim, P. Kathail, A. J. Carr, C. Burdziak, K. R. Moon, C. L. Chaffer, D. Pattabiraman, B. Bierie, L. Mazutis, G. Wolf, S. Krishnaswamy, D. Pe'er, Recovering gene interactions from single-cell data using data diffusion. *Cell* **174**, 716–729.e27 (2018).

79. A. Butler, P. Hoffman, P. Smibert, E. Papalexi, R. Satija, Integrating single-cell transcriptomic data across different conditions, technologies, and species. *Nat. Biotechnol.* **36**, 411–420 (2018).

80. F. A. Wolf, P. Angerer, F. J. Theis, SCANPY: Large-scale single-cell gene expression data analysis. *Genome Biol.* **19**, 15 (2018).

Science Immunology

Early precursors and molecular determinants of tissue-resident memory CD8$^+$ T lymphocytes revealed by single-cell RNA sequencing

Nadia S. Kurd, Zhaoren He, Tiani L. Louis, J. Justin Milner, Kyla D. Omilusik, Wenhao Jin, Matthew S. Tsai, Christella E. Widjaja, Jad N. Kanbar, Jocelyn G. Olvera, Tiffani Tysl, Lauren K. Quezada, Brigid S. Boland, Wendy J. Huang, Cornelis Murre, Ananda W. Goldrath, Gene W. Yeo and John T. Chang

Stepping down resident memory lane

The antigen-specific CD8$^+$ T response to microbial infection includes the differentiation of a subset of CD8$^+$ T cells into tissue-resident memory (T$_{RM}$) cells that stop circulating and become confined within a nonlymphoid tissue. Kurd *et al.* used single-cell RNA sequencing of mouse CD8$^+$ T cells at multiple time points during the first 90 days after viral infection to characterize how this differentiation process unfolds in the small intestine and tracks the emergence of heterogeneity among T$_{RM}$ cells. They found evidence for T$_{RM}$ cell precursors in the intestine by 4 days after infection and identified several putative regulators of T$_{RM}$ cell differentiation. The results of this study provide a valuable transcriptomic atlas that will facilitate further investigation into immune functions provided by T$_{RM}$ cells.

ARTICLE TOOLS	http://immunology.sciencemag.org/content/5/47/eaaz6894
SUPPLEMENTARY MATERIALS	http://immunology.sciencemag.org/content/suppl/2020/05/11/5.47.eaaz6894.DC1
REFERENCES	This article cites 79 articles, 18 of which you can access for free http://immunology.sciencemag.org/content/5/47/eaaz6894#BIBL
PERMISSIONS	http://www.sciencemag.org/help/reprints-and-permissions

Use of this article is subject to the Terms of Service